

## 7. SITE 907 (REVISITED)<sup>1,2</sup>

### Shipboard Scientific Party<sup>3</sup>

#### HOLE 907A

**Position:** 69°14.989'N, 12°41.894'W

**Start hole:** 1045 hr, 5 August 1993

**End hole:** 0400 hr, 8 August 1993

**Time on hole:** 65.25 hr (2.72 days)

**Seafloor (drill pipe measurement from rig floor, mbrf):** 1811.6

**Total depth (drill pipe measurement from rig floor, mbrf):** 2035.7

**Distance between rig floor and sea level (m):** 10.8

**Water depth (drill pipe measurement from sea level, m):** 1800.8

**Penetration (mbsf):** 224.1

**Coring totals:**

Type: APC

Number: 23

Cored: 216.3 m

Recovered: 225.10 m, 104.1%

Type: XCB

Number: 3

Cored: 7.8 m

Recovered: 4.88 m, 62.6%

**Total:**

Number: 26

Cored: 224.1 m

Recovered: 229.98 m, 102.6%

**Formation:**

Unit I: 0–16.8 mbsf; Pleistocene; silty clay, clayey silt, nannofossils, dropstones

Unit II: 16.8–56.3 mbsf; Pleistocene to Pliocene; clayey silt, silty clay, dropstones

Unit III: 56.3–118.1 mbsf; Pliocene to late Miocene; clayey silt, silty clay, biosilica, volcanic ash, dropstones

Unit IV: 118.1–197.3 mbsf; late to middle Miocene; silty clay and clayey silt; ash, biosilica

Unit V: 197.3–216.3 mbsf; middle Miocene; clayey mud, silty clay, biosilica

#### HOLE 907B

**Position:** 69°14.989'N, 12°41.898'W

**Start hole:** 2345 hr, 31 July 1995

**End hole:** 1915 hr, 1 August 1995

**Time on hole:** 19.5 hr (0.81 days)

**Seafloor (drill pipe measurement from rig floor, mbrf):** 1812.8

**Total depth (drill pipe measurement from rig floor, mbrf):** 2024.5

**Distance between rig floor and sea level (m):** 11.2

**Water depth (drill pipe measurement from sea level, m):** 1801.6

**Penetration (mbsf):** 211.7

**Coring totals:**

Type: APC

Number: 23

Cored: 211.7 m

Recovered: 219.56 m, 103.8%

**Formation:**

Unit I: 0–15.6 mbsf; Holocene to Pleistocene; clayey nannofossil mixed sediment, silty clay; clay with silt

Unit II: 15.6–63.1; Pleistocene to middle Pliocene; silty clay, clay with silt and ash, clay

Unit III: 63.1–196.1 mbsf; middle Pliocene to middle Miocene; silty clay, clay with silt, clay, and clay with diatoms

Unit IV: 196.1–214.9 mbsf; middle Miocene; silty clay, clay with silt, clay

#### HOLE 907C

**Position:** 69°14.998'N, 12°41.900'W

**Start hole:** 1915 hr, 1 August 1995

**End hole:** 1445 hr, 2 August 1995

**Time on hole:** 19.5 hr (0.81 days)

**Seafloor (drill pipe measurement from rig floor, mbrf):** 1812.4

**Total depth (drill pipe measurement from rig floor, mbrf):** 2027.5

**Distance between rig floor and sea level (m):** 11.2

**Water depth (drill pipe measurement from sea level, m):** 1801.2

**Penetration (mbsf):** 215.1

**Coring totals:**

Type: APC

Number: 23

Cored: 215.1 m

Recovered: 220.23 m, 102.4%

**Formation:**

Unit I: 0–15.6 mbsf; Holocene to Pleistocene; clayey nannofossil mixed sediment, silty clay; clay with silt

Unit II: 15.6–63.1 mbsf; Pleistocene to middle Pliocene; silty clay, clay with silt and ash, clay

Unit III: 63.1–196.1 mbsf; Pliocene to middle Miocene; silty clay, clay with silt, clay, and clay with diatoms

Unit IV: 196.1–214.9 mbsf; middle Miocene; silty clay, clay with silt, clay

**Principal results:** High-resolution shipboard multisensor track (MST) and color reflectance data document the continuity of the recovered section. A complete sediment sequence is documented for almost the entire section to 215 mbsf, and a continuous spliced section was constructed for high-resolution paleoclimate studies. It was also possible to establish a spliced composite section combining the MST records from Legs 151 and 162, thereby providing splices to fill in recovery gaps over core breaks for

<sup>1</sup>Jansen, E., Raymo, M.E., Blum, P., et al., 1996. *Proc. ODP, Init. Repts.*, 162: College Station, TX (Ocean Drilling Program).

<sup>2</sup>The first hole was drilled during Leg 151.

<sup>3</sup>Shipboard Scientific Party is given in the list preceding the Table of Contents.

high-resolution paleoclimate studies already underway on the sediments recovered at this site on Leg 151. These results document that the leg achieved the main objective of drilling Site 907.

The scarcity of biogenic material in certain intervals reduce the possibility of biostratigraphic age control, whereas a relatively clean magnetic polarity sequence enables correlation with confidence to the geomagnetic polarity time scale back to the upper Miocene, and with somewhat less confidence further back to approximately 16 Ma. Two short hiatuses or condensed intervals are indicated in the middle to late Miocene section. Indications of breaks at these intervals are supported by changes in sediment physical properties. Sedimentation rates average 17 m/m.y. over the last 3 Ma, 11 m/m.y. in the 3–5.5-Ma interval, and 22 m/m.y. in the 5.5–11-Ma interval.

The sediments at Site 907 are dominantly composed of silty clay, clay with silt, and clayey mixed sediment with varying amounts of biogenic material. The biogenic component, which includes calcareous nannofossils, foraminifers, diatoms, and/or spicules, is highly variable with depth. The bulk calcium carbonate content at this site displays high amplitude variations from near 0% to greater than 50% within the upper 100 mbsf depth. Below this level the sediments, for the most part, are carbonate-free. Dropstones greater than 1 cm in size are present upward from 62.9 mbsf. Ash layers and ash pods are abundant throughout Site 907 sediments. Four distinct lithostratigraphic units are defined with unit boundaries at 16, 63, and 196 mbsf.

Lithostratigraphic Unit I (0–15.6 mbsf; Holocene to Pleistocene) is primarily defined by the presence of relatively abundant calcareous microfossils, and high amplitude fluctuations in spectral reflectance. The sediment is predominantly alternating layers of clayey nannofossil mixed sediment with silty clay and clay with silt. Quartz, feldspar, and inorganic calcite are the most common terrigenous silt-sized particles. The pervasive colors of this unit are olive brown and olive gray, broken only by thin, darker volcanic ash layers.

Unit II (15.6–63.1 mbsf; middle Pleistocene to Pliocene) is characterized by the absence of biogenic sediment. The dominant lithologies include silty clay, clay with silt and ash, and clay. The sediments are predominantly composed of clay, quartz, feldspar, mica, and accessory minerals. Unit II, as well as Unit I, contains higher amounts of quartz, feldspar, and mica than are found in deeper intervals. Dark greenish gray, dark gray, and greenish gray-colored sediments are pervasive, although minor gray to black volcanic ash layers occur intermittently. Terrigenous components such as quartz and feldspar are relatively invariant across the boundary of Units I and II, in contrast to the downsection disappearance of biogenic material.

Unit III (63.1–196.1 mbsf; middle Pliocene to middle Miocene) is defined by the re-occurrence of biogenic sediment, in this case, biogenic silica, throughout the unit, with minor calcareous materials occurring within the uppermost section. The primary lithologies of Unit III are dark greenish gray to very dark greenish gray silty clay, clay with silt, clay, and clay with diatoms. With the exception of one small interval containing more than 55% nannofossils, Unit III is characterized by the minor repeated occurrence of biogenic material, primarily siliceous, which increases downcore from less than 5% at the upper boundary, to 5%–20% in the lower portion of the unit.

The major lithologies in Unit IV (196.1–214.9 mbsf; middle Miocene) are dark greenish gray to greenish gray silty clay, and clay with silt and clay. No biogenic sediment is found throughout the unit except for trace amounts of siliceous microfossils within the upper portion of the unit. The coarse fraction of Unit IV is similar to Unit III, but slightly lower amounts of quartz and higher amounts of sulfides.

Biogenic material occurs sporadically and intermittently throughout the sequence. It includes both calcareous and siliceous in Unit I and predominantly siliceous material in Unit III. The alternating biogenic-bearing and nonbiogenic sediments may reflect climatically driven changes over the Neogene. Shorter-term changes in oceanographic conditions are superimposed on this long-term variation, as the abundance of biogenic components occurring with Units I and III vary markedly within each unit. The boundary of Unit II and III may reflect the most important switch in

climatic and oceanic conditions associated with the onset of increased glaciation during the Pliocene. Quartz and feldspar increase markedly upsection at this level, dropstones first occur, and changes in the suite of clay minerals are indicated by changing natural gamma-ray emissions. Diminished accumulation of biogenic sediments subsequent to this boundary may reflect an overall environmental degradation, while barren intervals within Unit I may be more linked to high-amplitude climatic cycles within the late Pleistocene. Increased content of siliceous microfossils are reflected by lower density and higher porosity of the sediments of Unit III, compared with the more siliciclastic sediments of overlying Units I and II.

The geochemistry of the sedimentary sequence is characterized by processes typical of sulfate reduction and processes reflecting alteration of volcanic ash within the sediments and basement basalts below. Organic carbon values are generally low, but are highest in the intervals with the highest content of siliceous microfossils. Most geochemical parameters correlate well with Leg 151 results except those involved in sediment biodegradation processes. Leg 151 sulfate values from Hole 907A are substantially higher than those of Holes 907B and 907C in certain intervals. Whether this reflects lateral discontinuity or analytical differences remains to be determined.

## BACKGROUND AND OBJECTIVES

The drill sites on the Iceland Plateau (Sites 907 and 985) are part of a paleoenvironmental transect from Norway to Greenland designed to study the history of the advection of temperate, saline Atlantic waters into the Norwegian Sea (the “Nordic heat pump”), the position of the mixing front between these warm waters and the cold, partly ice-covered Arctic waters (the Arctic Front), and the position of the front delimiting the less saline, ice-covered Polar Waters of the East Greenland Current farther to the west. This transect, therefore, covers the climatically sensitive and variable thermal gradient between polar areas near east Greenland and temperate areas off Norway. Convection to intermediate depths in the Iceland Sea produces and modifies deep waters in the Nordic Seas, which are then a significant contributor to overflow waters across the Greenland-Scotland Ridge (the Southern Gateway) (Aagaard et al., 1985; Aagaard and Carmack, 1994; see fig. 8, chapter 1, this volume). Sites drilled on the Vøring Plateau during ODP Leg 104 (Eldholm, Thiede, Taylor, et al., 1987; Eldholm et al., 1989) anchor the eastern end of the transect, and site 987 (EGM-4) on the Greenland continental margin forms its western end (see Fig. 1). Site 907 is located between these end-members. The records from this site are intended to (1) monitor the history of oceanic and climatic fronts moving east and west across the Iceland Plateau, (2) derive an open-ocean record of ice-rafted debris (IRD) and carbonate accumulation, and (3) document the history of formation of northern-source deep waters.

Piston and ODP cores from this area document that warm phases were short, variable, and seldom occurred in the late Quaternary. In addition, each interglacial was very different from the others in terms of ocean circulation and the amount of heat advected to the region (Henrich and Baumann, 1994; Eide et al., in press). By extending this late Quaternary record back in time by drilling, we will be able to obtain a clearer picture of the long-term evolution of these short interglacial warm water spells. This will enable a clearer understanding of the relationships between the Nordic heat pump, ocean circulation patterns, and the glaciation history, on Milankovitch time scales. This will also provide insight into the climatic sensitivity of the Nordic Seas and their possible role as an early responder to orbital climate forcing (Imbrie et al., 1992, 1993; Koç and Jansen, 1994). Due to its projected pelagic IRD sedimentation and good time control, Site 907 will also be a central site for monitoring the long-term evolution of glaciation on the neighboring continents.

Site 907 (Fig. 1) is located on the Iceland Plateau, a shallow plateau defined by the 1800-m contour, which gently increases in depth away from the spreading axis, the Kolbeinsey Ridge. The southeast-

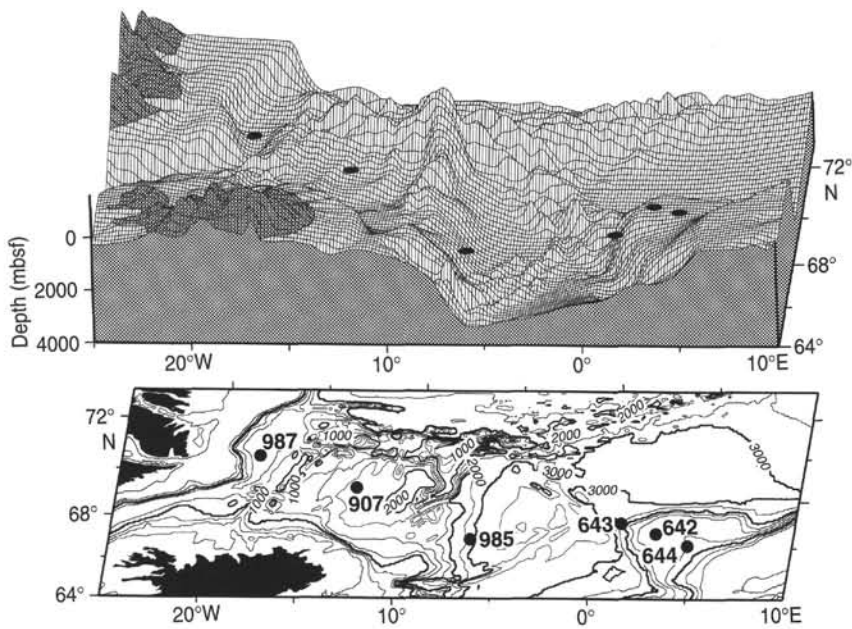


Figure 1. Bathymetry of the Nordic Seas paleoenvironmental transect, showing location of Legs 104, 151, and 162 drill sites. Bathymetric data (in meters) from ETOPOS.

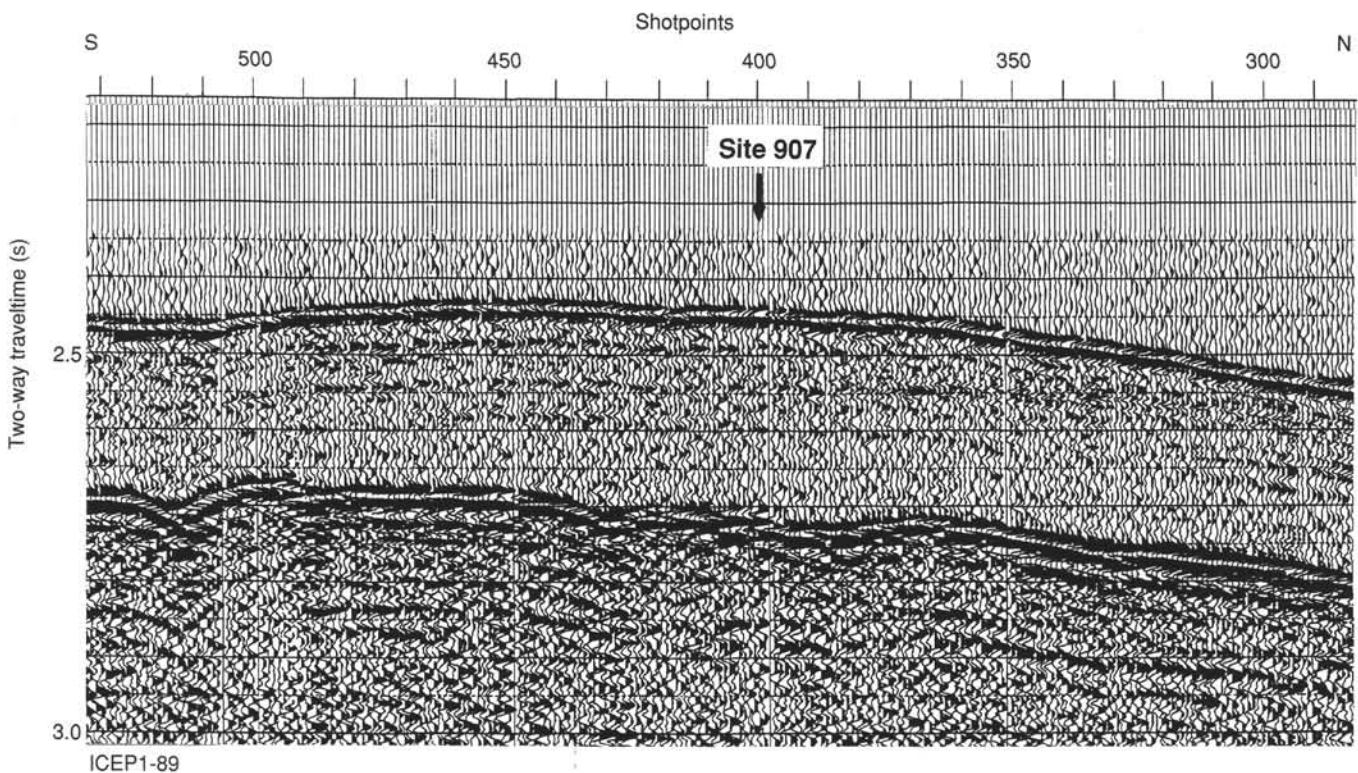


Figure 2. Seismic section through Site 907 (from Myhre, Thiede, Firth, et al., 1995).

ern part of the plateau drops off into the Norway Basin; to the south the plateau shallows toward the Iceland shelf. The northern boundary of the plateau is defined by the western segment of the Jan Mayen Fracture Zone, separating the plateau from the deeper Greenland Basin. Site 907 was drilled on what is believed to be Anomaly 6B crust (Eldholm and Windisch, 1974), between 22 and 24 Ma old. The Iceland Plateau is associated with an opaque, extremely smooth acoustic basement reflector, with only short, indistinct reflector elements observed below. Eldholm and Windisch (1974) suggested that real oce-

anic basement was buried beneath the opaque horizon, and that the opaque reflector represented a sill or dike body. The sedimentary sequence in the area can be divided into two major units: the uppermost sequence is characterized by weak, continuous, flat-lying reflectors, and the lower sequence is almost transparent (Myhre, Thiede, Firth, et al., 1995) (Fig. 2).

The primary objective of drilling operations at Site 907 was to recover an undisturbed pelagic sedimentary sequence. The site was expected to give an open-ocean record of IRD and carbonate, as it is

isolated from local continental influence. The site location also was chosen to find higher concentrations of calcareous pelagic fossils than were obtained at the previous DSDP and ODP sites in the Norwegian-Greenland Sea. ODP Leg 151 drilled one hole on Site 907 (Myhre, Thiede, Firth, et al., 1995). The remainder of the proposed three APC holes were not drilled due to a medical evacuation that discontinued operations on the site. Leg 162 reoccupied the site and drilled the two additional holes (Holes 907B and 907C).

The site location had been selected at shotpoint 400 of the ICEP1-89, Segment A multichannel seismic reflection line collected by the University of Bergen, Norway (Fig. 2). The Leg 151 site survey correlated with confidence the reflection data collected aboard the *JOIDES Resolution* to the pre-leg site-survey seismic profiles which, together with the 3.5-kHz record, suggested an undisturbed pelagic sedimentary sequence. Leg 162 therefore did not do a seismic survey, but drilled on the GPS position from Leg 151. During Leg 151, Hole 907A was APC-cored to 216.3 mbsf, where the core barrel bounced on what was shown to be a basaltic sequence. Drilling then continued with two XCB cores and achieved a total penetration of 224.1 mbsf; the last two cores were in basalt, after which the hole was logged (Myhre, Thiede, Firth, et al., 1995). The shipboard scientists on Leg 151 described five sedimentary units at Site 907 (Myhre, Thiede, Firth, et al., 1995):

- Unit I (0–16.8 mbsf), Pleistocene dark grayish brown to grayish brown clayey silts, silty clays, and foraminifer-bearing silty muds.
- Unit II (16.8–56.3 mbsf), Pliocene to Pleistocene clayey silts and silty clays.
- Unit III (56.3–118.1 mbsf), upper Miocene to Pliocene clayey silts and silty clays, with biogenic silica and volcanic glass.
- Unit IV (118.1–197.3 mbsf): middle to upper Miocene dark greenish gray to dark gray ash- and biosilica-bearing silty clays and clayey silts.
- Unit V (197.3–216.3 mbsf): middle Miocene dark olive gray clayey mud and silty clay, which is distinguished from Unit IV by its high quartz and clay and low biosilica contents.

Calcareous material is typically scarce. With the exception of a few thin nanofossil-rich horizons in the Pliocene, biocarbonate is restricted to the last 1 Ma. The site also has a clean magnetic polarity record although there is some uncertainty as to its correlation to the geomagnetic polarity time scale (see “Paleomagnetism” section, this chapter). According to the Leg 151 *Initial Reports* (Myhre, Thiede, Firth, et al., 1995), the objectives for Hole 907A were fulfilled in so far as the leg collected a more or less complete Neogene and Quaternary paleoenvironmental section. However, drilling at Site 907 did not fulfill expectations of obtaining extensive carbonate sedimentation records from the Neogene and Quaternary on the Iceland Plateau. Shore-based studies of the site have since provided a reliable stable isotope record of the last 1 Ma and a record of IRD, showing IRD deposition from surrounding continents back to more than 7 Ma, with major increases occurring at 6 Ma, 2.9 Ma, and 1 Ma (Fronval and Jansen, in press). Given that a detailed paleoclimatic record can be extracted from these sediments, it was desirable to return to the site and finish the planned triple coring to provide a complete and undisturbed high-latitude section for a large portion of the Neogene.

## OPERATIONS

The vessel covered the 625-nmi transit from Site 984 to Site 907 (ICEP-1) at an average speed of 11.9 kt. At 2249 hr the vessel slowed to survey speed (6.0 kt) and a short PDR acoustic profile was recorded across the site. The ship then returned to the site coordinates using the GPS.

Site 907 had initially been drilled during Leg 151. The first Hole 907A had contacted and penetrated a basalt sill at approximately 220 mbsf. In addition, Adara temperature measurements were taken during the piston-coring operation. The drilling plan for Leg 162 was to core two additional APC holes to construct a complete sediment section and provide additional sampling material. Since there was no interest in recovering the igneous contact, both holes were planned to terminate slightly above the total depth of Hole 907A.

At 0304 hr on 1 August 1995, the positioning beacon was deployed, initiating Hole 907B. A site location error in the prospectus of 3 min (1.5 nmi) to the east was discovered when the precision depth recorder showed nearly 100 m more water depth than at Hole 907A. The beacon was released and subsequently recovered and the vessel was offset in dynamic positioning mode to the correct site coordinates while pipe was being tripped.

A standard APC/XCB bottom-hole assembly (BHA) was used for all holes at Site 983, including a nonmagnetic drill collar. Holes 907B and 907C were offset 15 m to the north of Holes 907A and 907B, respectively. The mudline was established for each hole. The APC firing depth was offset by a few meters for subsequent holes to establish continuous sediment sections. Position, depths, and coring totals for each hole are summarized at the top of this chapter. All cores are listed in Table 1.

Routine piston coring proceeded without incident at Holes 907B and 907C until the scientific target depths had been reached. All cores beginning with Cores 907B-3H and 907C-3H, respectively, were oriented using the Tensor tool. The positioning beacon was released and subsequently recovered at 1138 hr on 2 August 1995, and the vessel was secured for transit and got underway for Site 985.

## COMPOSITE DEPTHS

Based on correlations between magnetic susceptibility, natural gamma radiation, and gamma-ray attenuation porosity (GRAPE) data, continuity of the sedimentary sequence was documented for most of the sequence drilled at Site 907, extending from the middle Miocene through the Holocene. The overlap of cores from Holes 907A, 907B, and 907C allowed a composite depth section to be constructed, as described in the “Composite Depths” section, “Explanatory Notes” chapter (this volume). The depth offsets that comprise the composite depth section for Site 907 are given in Table 2. Continuity of the sequence was achieved from the mudline to approximately 57.5 mcd, at the base of Core 162-907A-6H (57.55 mcd) and the base of Core 162-907C-6H (56.23 mcd), where overlap between adjacent holes was not maintained owing to high disturbance in Core 162-907B-7H. Below this depth, continuity of the stratigraphic section was again maintained to approximately 232 mcd (216 mbsf in Hole 907A, 212 mbsf in Hole 907B, and 215 mbsf in Hole 907C).

Multisensor track (MST) records that were useful in correlation are displayed on the composite depth scales in Figure 3 (see also back pocket). High-amplitude magnetic susceptibility and GRAPE (density) variations were used to determine depth offsets for the composite depth section, although magnetic susceptibility measurements at Hole 907A, drilled during Leg 151, were taken at lower resolution (8–10 cm) than at Holes 907B and 907C (~3 cm). At Holes 907B and 907C, *P*-wave velocity and natural gamma radiation measurements were collected over the entire cored sequence.

Although overlap between adjacent holes and relative agreement of sedimentary features in adjacent holes was excellent through most of the section, stretching and compression within the cored sequence occurred over most intervals. Because much of this distortion occurs on a scale of less than 9 m, it was not possible to align every sedimentary feature using only composite depth scale adjustments. Within-core, decimeter to centimeter depth scale adjustments would be required to align all sedimentary features simultaneously.

Table 1. Coring summary for Site 907.

Core	Date (Aug. 1995)	Time (UTC)	Depth (mbsf)	Length cored (m)	Length recovered (m)	Recovery (%)
162-907B-						
1H	1	0610	0.0-2.7	2.7	2.67	98.9
2H	1	0640	2.7-12.2	9.5	10.01	105.3
3H	1	0715	12.2-21.7	9.5	9.90	104.0
4H	1	0755	21.7-31.2	9.5	9.88	104.0
5H	1	0830	31.2-40.7	9.5	9.92	104.0
6H	1	0910	40.7-50.2	9.5	9.95	105.0
7H	1	0945	50.2-59.7	9.5	9.95	105.0
8H	1	1015	59.7-69.2	9.5	9.79	103.0
9H	1	1050	69.2-78.7	9.5	9.79	103.0
10H	1	1125	78.7-88.2	9.5	9.82	103.0
11H	1	1205	88.2-97.7	9.5	9.73	102.0
12H	1	1235	97.7-107.2	9.5	9.85	103.0
13H	1	1305	107.2-116.7	9.5	9.88	104.0
14H	1	1335	116.7-126.2	9.5	9.99	105.0
15H	1	1405	126.2-135.7	9.5	9.84	103.0
16H	1	1440	135.7-145.2	9.5	9.66	101.0
17H	1	1515	145.2-154.7	9.5	9.89	104.0
18H	1	1545	154.7-164.2	9.5	9.74	102.0
19H	1	1615	164.2-173.7	9.5	9.93	104.0
20H	1	1650	173.7-183.2	9.5	9.81	103.0
21H	1	1725	183.2-192.7	9.5	10.03	105.6
22H	1	1750	192.7-202.2	9.5	9.65	101.0
23H	1	1830	202.2-211.7	9.5	9.88	104.0
Coring totals:				211.7	219.60	103.7
162-907C-						
1H	1	2025	0.0-6.1	6.1	6.10	100.0
2H	1	2050	6.1-15.6	9.5	9.79	103.0
3H	1	2120	15.6-25.1	9.5	8.64	90.9
4H	1	2150	25.1-34.6	9.5	9.91	104.0
5H	1	2220	34.6-44.1	9.5	9.75	102.0
6H	1	2250	44.1-53.6	9.5	9.88	104.0
7H	1	2315	53.6-63.1	9.5	9.70	102.0
8H	1	2345	63.1-72.6	9.5	9.82	103.0
9H	2	0020	72.6-82.1	9.5	9.88	104.0
10H	2	0055	82.1-91.6	9.5	9.77	103.0
11H	2	0140	91.6-101.1	9.5	9.89	104.0
12H	2	0220	101.1-110.6	9.5	9.80	103.0
13H	2	0255	110.6-120.1	9.5	9.76	103.0
14H	2	0330	120.1-129.6	9.5	9.76	103.0
15H	2	0405	129.6-139.1	9.5	9.81	103.0
16H	2	0445	139.1-148.6	9.5	9.79	103.0
17H	2	0530	148.6-158.1	9.5	9.83	103.0
18H	2	0605	158.1-167.6	9.5	9.81	103.0
19H	2	0640	167.6-177.1	9.5	9.83	103.0
20H	2	0720	177.1-186.6	9.5	9.91	104.0
21H	2	0755	186.6-196.1	9.5	9.79	103.0
22H	2	0835	196.1-205.6	9.5	9.58	101.0
23H	2	0920	205.6-215.1	9.5	9.30	97.9
Coring totals:				215.1	220.20	102.4

The expansion of the composite depth section relative to the mbsf depth scale results from physical expansion of the cores after recovery as well as stretching of the sequence during the coring process. This expansion is illustrated in Figure 4. Growth of the mcd scale relative to the mbsf scale is less than 10% in the top half of all holes from Site 907. The overall expansion of the composite depth scale at Site 907 is slightly less than at the sites south of Iceland (Sites 980, 981, 982, 983, and 984).

Following construction of the composite depth section for Site 907, two spliced records were assembled from the aligned cores, as described in the "Explanatory Notes" chapter (this volume). Because Hole 907A was sampled at high resolution during Leg 151, two spliced records are desirable for Site 907, one which makes use of Hole 907A whenever possible, and another that is based primarily on Holes 907B and 907C. The advantage of two splices is that the first allows sedimentological data from Hole 907A to be incorporated into a single spliced record, while the second maximizes use of the much higher resolution MST and reflectance data collected on Leg 162. Either of these spliced records can be used as a sampling guide to recover an uninterrupted sedimentary sequence from Site 907. However, the "907A splice" is based on alignment of lower resolution MST records from Hole 907A with higher resolution records from Holes 907B and 907C, and thus it has an uncertainty of  $\pm 10$  cm in the mcd of splice tie points. The "907B/C splice," on the other

hand, has composite depths aligned so that tie points between adjacent holes are at exactly the same depth in meters composite depth. The tie points for the "907A splice" and the "907B/C splice" are given in Tables 3 and 4, respectively. Spliced magnetic susceptibility, natural gamma radiation, and GRAPE wet bulk density for the "907A splice" and the "907B/C splice" are shown in Figures 5 and 6.

## LITHOSTRATIGRAPHY

The sediments at Site 907 are dominantly composed of silty clay, clay with silt, and clayey mixed sediment with varying amounts of biogenic material. The biogenic component, which includes calcareous nannofossils, foraminifers, diatoms, and/or spicules, varies with depth, and its presence is one criterion used to delineate lithostratigraphic units. The bulk calcium carbonate content at this site displays high amplitude variations from near 0% to greater than 50% within the upper 100 mbsf. Below this level the sediments, for the most part, are carbonate-free (see "Organic Geochemistry" section, this chapter). Two sets of colors occur which are probably related at least partially to carbonate content. Olive brown and olive gray sediments are found only in the uppermost cores (Unit I), whereas dark greenish gray and very dark greenish gray sediments prevail throughout the remaining cores, with many minor gradational variations. Slight to moderate bioturbation is common at all depths. A total of 35 dropstones greater than 1.0 cm in size are present in Sections 162-907B-1H-1 through 6H-5 and 162-907C-1H-1 through 7H-6 (Fig. 7; Table 5). Ash layers and ash pods are abundant throughout Site 907 sediments.

Four distinct units are defined on the basis of the following seven criteria: (1) visual core description, (2) smear slide examination, (3) bulk calcium carbonate contents, (4) spectral reflectance, (5) magnetic susceptibility measurements, (6) natural gamma-ray measurements, and (7) X-ray diffraction analysis. Two biogenic-rich units (Units I and III) alternate with two long intervals of microfossil barren terrigenous sediment (Units II and IV). The four units are described in the next section. A summary of each lithostratigraphic unit is shown in Table 6.

### Description of Lithostratigraphic Units

#### Unit I

##### Intervals:

Core 162-907B-1H through Section 3H-3

Cores 162-907C-1H through 2H

Age: Holocene to Pleistocene

Depth: 0 to 15.6 mbsf

Lithostratigraphic Unit I is primarily defined by the presence of relatively abundant calcareous microfossils and by high amplitude fluctuations in spectral reflectance. A small siliceous component is present in the uppermost portion (Section 907A-1H-1). The sediment is dominated by alternating layers of clayey nannofossil mixed sediment with silty clay and clay with silt. Quartz, feldspar, and inorganic calcite are the most common terrigenous silt-sized particles. The pervasive colors of this unit are olive brown and olive gray, broken only by thin, dark volcanic ash layers. Subtle, gradational color changes occur throughout the unit. The gradational nature of the color changes is attributed to the ubiquitous bioturbation.

Several distinct sediment types are observed in Unit I. Two coarse-grained sediment layers are present in intervals 907B-2H-6, 107-110 cm, and 141-142 cm, at depths of 7.2 and 11.3 mbsf, respectively (Fig. 8). Numerous dropstones and volcanic ash layers are scattered throughout (Table 5). High amplitude fluctuations and a downcore trend of decreasing average values in percentage spectral reflectance (red band, 650-700 nm) are observed in Unit I, as well. Magnetic susceptibility and natural gamma radiation values show slight fluctuation, but no trend within Unit I.

Table 2. Site 907 composite depths.

Core, section	Length (cm)	Depth (mbsf)	Depth (mcd)	Offset (mcd – mbsf)	Core, section	Length (cm)	Depth (mbsf)	Depth (mcd)	Offset (mcd – mbsf)
162-907A-					12H-4	150	106.80	112.68	5.88
1H-1	150	0.00	0.00	0.00	12H-5	150	108.30	114.18	5.88
1H-2	150	1.50	1.50	0.00	12H-6	150	109.80	115.68	5.88
1H-3	150	3.00	3.00	0.00	12H-7	67	111.30	117.18	5.88
1H-4	150	4.50	4.50	0.00	12H-CC	30	111.97	117.85	5.88
1H-5	100	6.00	6.00	0.00	13H-1	150	111.80	119.52	7.72
1H-CC	27	7.00	7.00	0.00	13H-2	150	113.30	121.02	7.72
2H-1	150	7.30	7.33	0.03	13H-3	150	114.80	122.52	7.72
2H-2	150	8.80	8.83	0.03	13H-4	150	116.30	124.02	7.72
2H-3	150	10.30	10.33	0.03	13H-5	150	117.80	125.52	7.72
2H-4	150	11.80	11.83	0.03	13H-6	150	119.30	127.02	7.72
2H-5	150	13.30	13.33	0.03	13H-7	82	120.80	128.52	7.72
2H-6	150	14.80	14.83	0.03	13H-CC	18	121.62	129.34	7.72
2H-7	56	16.30	16.33	0.03	14H-1	150	121.30	128.61	7.31
2H-CC	25	16.86	16.89	0.03	14H-2	150	122.80	130.11	7.31
3H-1	150	16.80	18.30	1.50	14H-3	150	124.30	131.61	7.31
3H-2	150	18.30	19.80	1.50	14H-4	150	125.80	133.11	7.31
3H-3	150	19.80	21.30	1.50	14H-5	150	127.30	134.61	7.31
3H-4	150	21.30	22.80	1.50	14H-6	150	128.80	136.11	7.31
3H-5	150	22.80	24.30	1.50	14H-7	68	130.30	137.61	7.31
3H-6	150	24.30	25.80	1.50	14H-CC	25	130.98	138.29	7.31
3H-7	46	25.80	27.30	1.50	15H-1	150	130.80	139.39	8.59
3H-CC	40	26.26	27.76	1.50	15H-2	150	132.30	140.89	8.59
4H-1	150	26.30	29.03	2.73	15H-3	150	133.80	142.39	8.59
4H-2	150	27.80	30.53	2.73	15H-4	150	135.30	143.89	8.59
4H-3	150	29.30	32.03	2.73	15H-5	153	136.80	145.39	8.59
4H-4	150	30.80	33.53	2.73	15H-6	150	138.33	146.92	8.59
4H-5	150	32.30	35.03	2.73	15H-7	42	139.83	148.42	8.59
4H-6	150	33.80	36.53	2.73	15H-CC	28	140.25	148.84	8.59
4H-7	73	35.30	38.03	2.73	16H-1	150	140.30	149.35	9.05
4H-CC	20	36.03	38.76	2.73	16H-2	150	141.80	150.85	9.05
5H-1	150	35.80	40.73	4.93	16H-3	150	143.30	152.35	9.05
5H-2	150	37.30	42.23	4.93	16H-4	150	144.80	153.85	9.05
5H-3	150	38.80	43.73	4.93	16H-5	150	146.30	155.35	9.05
5H-4	150	40.30	45.23	4.93	16H-6	150	147.80	156.85	9.05
5H-5	150	41.80	46.73	4.93	16H-7	61	149.30	158.35	9.05
5H-6	150	43.30	48.23	4.93	16H-CC	31	149.91	158.96	9.05
5H-7	85	44.80	49.73	4.93	17H-1	150	149.80	159.55	9.75
5H-CC	25	45.65	50.58	4.93	17H-2	150	151.30	161.05	9.75
6H-1	150	45.30	47.84	2.54	17H-3	150	152.80	162.55	9.75
6H-2	150	46.80	49.34	2.54	17H-4	150	154.30	164.05	9.75
6H-3	150	48.30	50.84	2.54	17H-5	150	155.80	165.55	9.75
6H-4	150	49.80	52.34	2.54	17H-6	150	157.30	167.05	9.75
6H-5	150	51.30	53.84	2.54	17H-7	74	158.80	168.55	9.75
6H-6	150	52.80	55.34	2.54	17H-CC	27	159.54	169.29	9.75
6H-7	71	54.30	56.84	2.54	18H-1	150	159.30	170.79	11.49
6H-CC	35	55.01	57.55	2.54	18H-2	150	160.80	172.29	11.49
7H-1	150	54.80	58.06	3.26	18H-3	150	162.30	173.79	11.49
7H-2	150	56.30	59.56	3.26	18H-4	150	163.80	175.29	11.49
7H-3	150	57.80	61.06	3.26	18H-5	150	165.30	176.79	11.49
7H-4	150	59.30	62.56	3.26	18H-6	150	166.80	178.29	11.49
7H-5	150	60.80	64.06	3.26	18H-7	60	168.30	179.79	11.49
7H-6	150	62.30	65.56	3.26	18H-CC	27	168.90	180.39	11.49
7H-7	64	63.80	67.06	3.26	19H-1	150	168.80	183.03	14.23
7H-CC	26	64.44	67.70	3.26	19H-2	150	170.30	184.53	14.23
8H-1	150	64.30	68.56	4.26	19H-3	150	171.80	186.03	14.23
8H-2	150	65.80	70.06	4.26	19H-4	150	173.30	187.53	14.23
8H-3	150	67.30	71.56	4.26	19H-5	150	174.80	189.03	14.23
8H-4	150	68.80	73.06	4.26	19H-6	150	176.30	190.53	14.23
8H-5	150	70.30	74.56	4.26	19H-7	75	177.80	192.03	14.23
8H-6	150	71.80	76.06	4.26	19H-CC	24	178.55	192.78	14.23
8H-7	55	73.30	77.56	4.26	20H-1	150	178.30	193.03	14.73
8H-CC	27	73.85	78.11	4.26	20H-2	150	179.80	194.53	14.73
9H-1	150	73.80	78.18	4.38	20H-3	150	181.30	196.03	14.73
9H-2	150	75.30	79.68	4.38	20H-4	150	182.80	197.53	14.73
9H-3	150	76.80	81.18	4.38	20H-5	150	184.30	199.03	14.73
9H-4	150	78.30	82.68	4.38	20H-6	150	185.80	200.53	14.73
9H-5	150	79.80	84.18	4.38	20H-7	60	187.30	202.03	14.73
9H-6	150	81.30	85.68	4.38	20H-CC	25	187.90	202.63	14.73
9H-7	81	82.80	87.18	4.38	21H-1	150	187.80	203.99	16.19
9H-CC	38	83.61	87.99	4.38	21H-2	150	189.30	205.49	16.19
10H-1	150	83.30	88.23	4.93	21H-3	150	190.80	206.99	16.19
10H-2	150	84.80	89.73	4.93	21H-4	150	192.30	208.49	16.19
10H-3	150	86.30	91.23	4.93	21H-5	150	193.80	209.99	16.19
10H-4	150	87.80	92.73	4.93	21H-6	150	195.30	211.49	16.19
10H-5	150	89.30	94.23	4.93	21H-7	58	196.80	212.99	16.19
10H-6	150	90.80	95.73	4.93	21H-CC	1	197.38	213.57	16.19
10H-7	71	92.30	97.23	4.93	22H-1	150	197.30	213.65	16.35
10H-CC	26	93.01	97.94	4.93	22H-2	150	198.80	215.15	16.35
11H-1	150	92.80	98.02	5.22	22H-3	150	200.30	216.65	16.35
11H-2	150	94.30	99.52	5.22	22H-4	150	201.80	218.15	16.35
11H-3	150	95.80	101.02	5.22	22H-5	150	203.30	219.65	16.35
11H-4	150	97.30	102.52	5.22	22H-6	150	204.80	221.15	16.35
11H-5	150	98.80	104.02	5.22	22H-7	55	206.30	222.65	16.35
11H-6	150	100.30	105.52	5.22	22H-CC	3	206.85	223.20	16.35
11H-7	84	101.80	107.02	5.22	23H-1	150	206.80	222.97	16.17
11H-CC	23	102.64	107.86	5.22	23H-2	150	208.30	224.47	16.17
12H-1	150	102.30	108.18	5.88	23H-3	150	209.80	225.97	16.17
12H-2	150	103.80	109.68	5.88	23H-4	150	211.30	227.47	16.17
12H-3	150	105.30	111.18	5.88	23H-5	150	212.80	228.97	16.17

Table 2 (continued).

Core, section	Length (cm)	Depth (mbsf)	Depth (mcd)	Offset (mcd - mbsf)	Core, section	Length (cm)	Depth (mbsf)	Depth (mcd)	Offset (mcd - mbsf)
23H-6	150	214.30	230.47	16.17	11H-6	150	95.70	102.33	6.63
23H-7	60	215.80	231.97	16.17	11H-7	50	97.20	103.83	6.63
23H-CC	18	216.40	232.57	16.17	11H-CC	23	97.70	104.33	6.63
24X-CC	53	216.30	232.47	16.17	12H-1	150	97.70	104.26	6.56
25X-1	138	217.30	233.47	16.17	12H-2	150	99.20	105.76	6.56
25X-2	150	218.68	234.85	16.17	12H-3	150	100.70	107.26	6.56
25X-3	23	220.18	236.35	16.17	12H-4	150	102.20	108.76	6.56
26X-1	144	221.00	237.17	16.17	12H-5	150	103.70	110.26	6.56
26X-2	92	222.44	238.61	16.17	12H-6	150	105.20	111.76	6.56
162-907B-					12H-7	62	106.70	113.26	6.56
1H-1	150	0.00	0.22	0.22	12H-CC	23	107.32	113.88	6.56
1H-2	100	1.50	1.72	0.22	13H-1	150	107.20	114.43	7.23
1H-CC	17	2.50	2.72	0.22	13H-2	150	108.70	115.93	7.23
2H-1	150	2.70	3.03	0.33	13H-3	150	110.20	117.43	7.23
2H-2	150	4.20	4.53	0.33	13H-4	150	111.70	118.93	7.23
2H-3	150	5.70	6.03	0.33	13H-5	150	113.20	120.43	7.23
2H-4	150	7.20	7.53	0.33	13H-6	150	114.70	121.93	7.23
2H-5	150	8.70	9.03	0.33	13H-7	64	116.20	123.43	7.23
2H-6	150	10.20	10.53	0.33	13H-CC	24	116.84	124.07	7.23
2H-7	73	11.70	12.03	0.33	14H-1	150	116.70	125.09	8.39
2H-CC	28	12.43	12.76	0.33	14H-2	150	118.20	126.59	8.39
3H-1	150	12.20	13.77	1.57	14H-3	150	119.70	128.09	8.39
3H-2	150	13.70	15.27	1.57	14H-4	150	121.20	129.59	8.39
3H-3	150	15.20	16.77	1.57	14H-5	150	122.70	131.09	8.39
3H-4	150	16.70	18.27	1.57	14H-6	150	124.20	132.59	8.39
3H-5	150	18.20	19.77	1.57	14H-7	74	125.70	134.09	8.39
3H-6	150	19.70	21.27	1.57	14H-CC	25	126.44	134.83	8.39
3H-7	70	21.20	22.77	1.57	15H-1	150	126.20	134.91	8.71
3H-CC	20	21.90	23.47	1.57	15H-2	150	127.70	136.41	8.71
4H-1	150	21.70	23.85	2.15	15H-3	150	129.20	137.91	8.71
4H-2	150	23.20	25.35	2.15	15H-4	150	130.70	139.41	8.71
4H-3	150	24.70	26.85	2.15	15H-5	150	132.20	140.91	8.71
4H-4	150	26.20	28.35	2.15	15H-6	150	133.70	142.41	8.71
4H-5	150	27.70	29.85	2.15	15H-7	60	135.20	143.91	8.71
4H-6	150	29.20	31.35	2.15	15H-CC	24	135.80	144.51	8.71
4H-7	63	30.70	32.85	2.15	16H-1	150	135.70	145.17	9.47
4H-CC	25	31.33	33.48	2.15	16H-2	150	137.20	146.67	9.47
5H-1	150	31.20	34.27	3.07	16H-3	150	138.70	148.17	9.47
5H-2	150	32.70	35.77	3.07	16H-4	42	140.20	149.67	9.47
5H-3	150	34.20	37.27	3.07	16H-5	150	140.62	150.09	9.47
5H-4	150	35.70	38.77	3.07	16H-6	150	142.12	151.59	9.47
5H-5	150	37.20	40.27	3.07	16H-7	150	143.62	153.09	9.47
5H-6	150	38.70	41.77	3.07	16H-CC	24	145.12	154.59	9.47
5H-7	68	40.20	43.27	3.07	17H-1	150	145.20	155.44	10.24
5H-CC	24	40.88	43.95	3.07	17H-2	150	146.70	156.94	10.24
6H-1	150	40.70	44.77	4.07	17H-3	150	148.20	158.44	10.24
6H-2	150	42.20	46.27	4.07	17H-4	150	149.70	159.94	10.24
6H-3	150	43.70	47.77	4.07	17H-5	150	151.20	161.44	10.24
6H-4	150	45.20	49.27	4.07	17H-6	150	152.70	162.94	10.24
6H-5	150	46.70	50.77	4.07	17H-7	64	154.20	164.44	10.24
6H-6	150	48.20	52.27	4.07	17H-CC	25	154.84	165.08	10.24
6H-7	64	49.70	53.77	4.07	18H-1	150	154.70	166.62	11.92
6H-CC	31	50.34	54.41	4.07	18H-2	150	156.20	168.12	11.92
7H-1	150	50.20	54.77	4.57	18H-3	150	157.70	169.62	11.92
7H-2	150	51.70	56.27	4.57	18H-4	150	159.20	171.12	11.92
7H-3	150	53.20	57.77	4.57	18H-5	150	160.70	172.62	11.92
7H-4	150	54.70	59.27	4.57	18H-6	150	162.20	174.12	11.92
7H-5	150	56.20	60.77	4.57	18H-7	61	163.70	175.62	11.92
7H-6	150	57.70	62.27	4.57	18H-CC	13	164.31	176.23	11.92
7H-7	70	59.20	63.77	4.57	19H-1	150	164.20	177.39	13.19
7H-CC	25	59.90	64.47	4.57	19H-2	150	165.70	178.89	13.19
8H-1	150	59.70	64.97	5.27	19H-3	150	167.20	180.39	13.19
8H-2	150	61.20	66.47	5.27	19H-4	150	168.70	181.89	13.19
8H-3	150	62.70	67.97	5.27	19H-5	150	170.20	183.39	13.19
8H-4	150	64.20	69.47	5.27	19H-6	150	171.70	184.89	13.19
8H-5	150	65.70	70.97	5.27	19H-7	68	173.20	186.39	13.19
8H-6	150	67.20	72.47	5.27	19H-CC	25	173.88	187.07	13.19
8H-7	56	68.70	73.97	5.27	20H-1	150	173.70	188.47	14.77
8H-CC	23	69.26	74.53	5.27	20H-2	150	175.20	189.97	14.77
9H-1	150	69.20	74.88	5.68	20H-3	150	176.70	191.47	14.77
9H-2	150	70.70	76.38	5.68	20H-4	150	178.20	192.97	14.77
9H-3	150	72.20	77.88	5.68	20H-5	150	179.70	194.47	14.77
9H-4	150	73.70	79.38	5.68	20H-6	150	181.20	195.97	14.77
9H-5	150	75.20	80.88	5.68	20H-7	56	182.70	197.47	14.77
9H-6	150	76.70	82.38	5.68	20H-CC	25	183.26	198.03	14.77
9H-7	55	78.20	83.88	5.68	21H-1	150	183.20	198.33	15.13
9H-CC	24	78.75	84.43	5.68	21H-2	150	184.70	199.83	15.13
10H-1	150	78.70	84.72	6.02	21H-3	150	186.20	201.33	15.13
10H-2	150	80.20	86.22	6.02	21H-4	150	187.70	202.83	15.13
10H-3	150	81.70	87.72	6.02	21H-5	150	189.20	204.33	15.13
10H-4	150	83.20	89.22	6.02	21H-6	150	190.70	205.83	15.13
10H-5	150	84.70	90.72	6.02	21H-7	79	192.20	207.33	15.13
10H-6	150	86.20	92.22	6.02	21H-CC	24	192.99	208.12	15.13
10H-7	60	87.70	93.72	6.02	22H-1	150	192.70	209.49	16.79
10H-CC	22	88.30	94.32	6.02	22H-2	150	194.20	210.99	16.79
11H-1	150	88.20	94.83	6.63	22H-3	150	195.70	212.49	16.79
11H-2	150	89.70	96.33	6.63	22H-4	150	197.20	213.99	16.79
11H-3	150	91.20	97.83	6.63	22H-5	150	198.70	215.49	16.79
11H-4	150	92.70	99.33	6.63	22H-6	150	200.20	216.99	16.79
11H-5	150	94.20	100.83	6.63	22H-7	44	201.70	218.49	16.79
					22H-CC	21	202.14	218.93	16.79

Table 2 (continued).

Core, section	Length (cm)	Depth (mbsf)	Depth (mcd)	Offset (mcd - mbsf)	Core, section	Length (cm)	Depth (mbsf)	Depth (mcd)	Offset (mcd - mbsf)
23H-1	150	202.20	219.72	17.52	11H-5	150	97.60	103.90	6.30
23H-2	150	203.70	221.22	17.52	11H-6	150	99.10	105.40	6.30
23H-3	150	205.20	222.72	17.52	11H-7	64	100.60	106.90	6.30
23H-4	150	206.70	224.22	17.52	11H-CC	25	101.24	107.54	6.30
23H-5	150	208.20	225.72	17.52	12H-1	150	101.10	107.93	6.83
23H-6	150	209.70	227.22	17.52	12H-2	150	102.60	109.43	6.83
23H-7	65	211.20	228.72	17.52	12H-3	150	104.10	110.93	6.83
23H-CC	23	211.85	229.37	17.52	12H-4	150	105.60	112.43	6.83
162-907C-					12H-5	150	107.10	113.93	6.83
1H-1	150	0.00	0.00	0.00	12H-6	150	108.60	115.43	6.83
1H-2	150	1.50	1.50	0.00	12H-7	56	110.10	116.93	6.83
1H-3	150	3.00	3.00	0.00	12H-CC	24	110.66	117.49	6.83
1H-4	140	4.50	4.50	0.00	13H-1	150	110.60	118.02	7.42
1H-CC	20	5.90	5.90	0.00	13H-2	150	112.10	119.52	7.42
2H-1	150	6.10	6.96	0.86	13H-3	150	113.60	121.02	7.42
2H-2	150	7.60	8.46	0.86	13H-4	150	115.10	122.52	7.42
2H-3	150	9.10	9.96	0.86	13H-5	150	116.60	124.02	7.42
2H-4	150	10.60	11.46	0.86	13H-6	150	118.10	125.52	7.42
2H-5	150	12.10	12.96	0.86	13H-7	65	119.60	127.02	7.42
2H-6	150	13.60	14.46	0.86	13H-CC	24	120.25	127.67	7.42
2H-7	56	15.10	15.96	0.86	14H-1	150	120.10	128.30	8.20
2H-CC	23	15.66	16.52	0.86	14H-2	150	121.60	129.80	8.20
3H-1	150	15.60	17.79	2.19	14H-3	150	123.10	131.30	8.20
3H-2	150	17.10	19.29	2.19	14H-4	150	124.60	132.80	8.20
3H-3	150	18.60	20.79	2.19	14H-5	150	126.10	134.30	8.20
3H-4	150	20.10	22.29	2.19	14H-6	150	127.60	135.80	8.20
3H-5	150	21.60	23.79	2.19	14H-7	54	129.10	137.30	8.20
3H-6	88	23.10	25.29	2.19	14H-CC	22	129.64	137.84	8.20
3H-CC	26	23.98	26.17	2.19	15H-1	150	129.60	138.90	9.30
4H-1	150	25.10	27.05	1.95	15H-2	150	131.10	140.40	9.30
4H-2	150	26.60	28.55	1.95	15H-3	150	132.60	141.90	9.30
4H-3	150	28.10	30.05	1.95	15H-4	150	134.10	143.40	9.30
4H-4	150	29.60	31.55	1.95	15H-5	150	135.60	144.90	9.30
4H-5	150	31.10	33.05	1.95	15H-6	150	137.10	146.40	9.30
4H-6	150	32.60	34.55	1.95	15H-7	57	138.60	147.90	9.30
4H-7	70	34.10	36.05	1.95	15H-CC	24	139.17	148.47	9.30
4H-CC	21	34.80	36.75	1.95	16H-1	150	139.10	149.13	10.03
5H-1	150	34.60	37.78	3.18	16H-2	150	140.60	150.63	10.03
5H-2	150	36.10	39.28	3.18	16H-3	150	142.10	152.13	10.03
5H-3	150	37.60	40.78	3.18	16H-4	150	143.60	153.63	10.03
5H-4	150	39.10	42.28	3.18	16H-5	150	145.10	155.13	10.03
5H-5	150	40.60	43.78	3.18	16H-6	150	146.60	156.63	10.03
5H-6	150	42.10	45.28	3.18	16H-7	58	148.10	158.13	10.03
5H-7	51	43.60	46.78	3.18	16H-CC	21	148.68	158.71	10.03
5H-CC	24	44.11	47.29	3.18	17H-1	150	148.60	159.87	11.27
6H-1	150	44.10	46.60	2.50	17H-2	150	150.10	161.37	11.27
6H-2	150	45.60	48.10	2.50	17H-3	150	151.60	162.87	11.27
6H-3	150	47.10	49.60	2.50	17H-4	150	153.10	164.37	11.27
6H-4	150	48.60	51.10	2.50	17H-5	150	154.60	165.87	11.27
6H-5	150	50.10	52.60	2.50	17H-6	150	156.10	167.37	11.27
6H-6	150	51.60	54.10	2.50	17H-7	60	157.60	168.87	11.27
6H-7	63	53.10	55.60	2.50	17H-CC	23	158.20	169.47	11.27
6H-CC	25	53.73	56.23	2.50	18H-1	150	158.10	169.88	11.78
7H-1	150	53.60	57.62	4.02	18H-2	150	159.60	171.38	11.78
7H-2	150	55.10	59.12	4.02	18H-3	150	161.10	172.88	11.78
7H-3	150	56.60	60.62	4.02	18H-4	150	162.60	174.38	11.78
7H-4	150	58.10	62.12	4.02	18H-5	150	164.10	175.88	11.78
7H-5	150	59.60	63.62	4.02	18H-6	150	165.60	177.38	11.78
7H-6	150	61.10	65.12	4.02	18H-7	60	167.10	178.88	11.78
7H-7	44	62.60	66.62	4.02	18H-CC	21	167.70	179.48	11.78
7H-CC	26	63.04	67.06	4.02	19H-1	150	167.60	181.11	13.50
8H-1	150	63.10	67.74	4.64	19H-2	150	169.10	182.61	13.50
8H-2	150	64.60	69.24	4.64	19H-3	150	170.60	184.11	13.50
8H-3	150	66.10	70.74	4.64	19H-4	150	172.10	185.61	13.50
8H-4	150	67.60	72.24	4.64	19H-5	150	173.60	187.11	13.50
8H-5	150	69.10	73.74	4.64	19H-6	150	175.10	188.61	13.50
8H-6	150	70.60	75.24	4.64	19H-7	63	176.60	190.11	13.50
8H-7	59	72.10	76.74	4.64	19H-CC	20	177.23	190.73	13.50
8H-CC	23	72.69	77.33	4.64	20H-1	150	177.10	191.31	14.20
9H-1	150	72.60	77.78	5.18	20H-2	150	178.60	192.81	14.20
9H-2	150	74.10	79.28	5.18	20H-3	150	180.10	194.30	14.20
9H-3	150	75.60	80.78	5.18	20H-4	150	181.60	195.80	14.20
9H-4	150	77.10	82.28	5.18	20H-5	150	183.10	197.30	14.20
9H-5	150	78.60	83.78	5.18	20H-6	150	184.60	198.80	14.20
9H-6	150	80.10	85.28	5.18	20H-7	65	186.10	200.30	14.20
9H-7	61	81.60	86.78	5.18	20H-CC	26	186.75	200.95	14.20
9H-CC	27	82.21	87.39	5.18	21H-1	150	186.60	202.07	15.47
10H-1	150	82.10	87.87	5.77	21H-2	150	188.10	203.57	15.47
10H-2	150	83.60	89.37	5.77	21H-3	150	189.60	205.07	15.47
10H-3	150	85.10	90.87	5.77	21H-4	150	191.10	206.57	15.47
10H-4	150	86.60	92.37	5.77	21H-5	150	192.60	208.07	15.47
10H-5	150	88.10	93.87	5.77	21H-6	150	194.10	209.57	15.47
10H-6	150	89.60	95.37	5.77	21H-7	60	195.60	211.07	15.47
10H-7	54	91.10	96.87	5.77	21H-CC	19	196.20	211.67	15.47
10H-CC	23	91.64	97.41	5.77	22H-1	150	196.10	212.72	16.62
11H-1	150	91.60	97.90	6.30	22H-2	150	197.60	214.22	16.62
11H-2	150	93.10	99.40	6.30	22H-3	150	199.10	215.72	16.62
11H-3	150	94.60	100.90	6.30	22H-4	150	200.60	217.22	16.62
11H-4	150	96.10	102.40	6.30	22H-5	150	202.10	218.72	16.62
					22H-6	150	203.60	220.22	16.62

Table 2 (continued).

Core, section	Length (cm)	Depth (mbsf)	Depth (mcd)	Offset (mcd - mbsf)
22H-7	58	205.10	221.72	16.62
23H-1	150	205.60	223.34	17.74
23H-2	150	207.10	224.84	17.74
23H-3	150	208.60	226.34	17.74
23H-4	150	210.10	227.84	17.74
23H-5	150	211.60	229.34	17.74
23H-6	150	213.10	230.84	17.74
23H-CC	30	214.60	232.34	17.74

Note: Depths are from the top of each section.

## Unit II

### Intervals:

Sections 162-907B-3H-3 through 8H-3

Cores 162-907C-3H through 7H

Age: Pleistocene to Pliocene

Depth: 15.6 to 63.1 mbsf

Unit II is characterized by the absence of biogenic sediment. The dominant lithologies include silty clay, clay with silt and ash, and clay. The sediments are predominantly composed of clay, quartz, feldspar, mica, and accessory minerals. The smear slide and XRD analyses reveal that Unit II, as well as Unit I, contains higher amounts of quartz, feldspar, and mica than deeper intervals (Units III and IV; Fig. 9). Dark greenish gray, dark gray, and greenish gray-colored sediments are pervasive, although minor gray to black volcanic ash layers occur intermittently. A small downcore increase in natural gamma emissions marks the top of Unit II, followed by a steep decrease toward the bottom of the unit. Dropstones continue to occur throughout Unit II (Fig. 7). Terrigenous components such as quartz and feldspar are relatively invariant across the boundary of Units I and II, in contrast to the disappearance of biogenic material.

## Unit III

### Intervals:

Sections 162-907B-8H-3 through 22H-3

Cores 162-907C-8H through 21H

Age: Pliocene to middle Miocene

Depth: 63.1 to 196.1 mbsf

The primary lithologies of Unit III are dark greenish gray to very dark greenish gray silty clay, clay with silt, clay, and clay with diatoms. Unit III is characterized by the re-occurrence of biogenic siliceous sediment, which is present throughout the unit. This biogenic siliceous sediment shows a slight increase downcore. The biogenic calcareous materials occur only in the uppermost sections of Unit III (Sections 907B-8H-2, 8H-3, and 907C-8H-1, 61.2–64.5 mbsf). The siliciclastic materials (volcanic ash, quartz, feldspar, mica, and accessory minerals) are relatively constant throughout the unit.

## Unit IV

### Intervals:

Section 162-907B-22H-3 through Core 23H

Cores 162-907C-22H through 23H

Age: middle Miocene

Depth: 196.1 to 214.9 mbsf

The major lithologies in Unit IV are dark greenish gray to greenish gray silty clay, clay with silt and clay. No biogenic sediment is found throughout the unit except for trace amounts of siliceous microfossils within the upper portion of the Unit. The coarse fraction of Unit IV is similar to Unit III, but with slightly lower amounts of quartz and higher amounts of sulfides. Magnetic susceptibility and

natural gamma radiation values display an increasing trend downcore from the boundary of Units III and IV.

## Interpretation

The four lithostratigraphic units are defined at Site 907 by the previously mentioned criteria (Table 6). Our interpretation is based primarily on the alternating biogenic and terrigenous sediment, and on compositional changes within the siliciclastic component.

Site 907 is located at the center of the Iceland Plateau, relatively distant from surrounding land masses. Open-ocean conditions are likely to have prevailed at this site since at least the middle Miocene (Talwani and Eldholm, 1977). Thus, the relatively low concentrations of biogenic material and recurrence of barren intervals cannot reflect the impact of near-shore processes such as sea-surface turbidity or riverine fresh water. In addition, dilution by terrigenous sediment, common in some near-shore environments as well as in particular deep-sea settings, is unlikely, considering the modest sedimentation rates throughout the recovered sequence (see "Sedimentation Rates" section, this chapter). The accumulation of biogenic sediment must be limited, therefore, by processes occurring at the sea surface (e.g., nutrient limitations, sea-ice cover, severe climatic conditions), or within the deep sea (e.g., selective removal by dissolution).

Biogenic material occurs sporadically and intermittently throughout the sequence, and switches from including both calcareous and siliceous material in Unit I to consisting almost exclusively of siliceous material in Unit III. The alternating biogenic-bearing and non-biogenic sediments may reflect climatically driven changes over the Neogene. Shorter-term changes in oceanographic and/or climatic conditions seem to be superimposed on this long-term variation as reflected by the variations in the abundance of biogenic components that occur within Units I and III. The boundary between Unit II and III may reflect an important switch in climatic and oceanic conditions, as the drop in biogenic content is accompanied by the onset of dropstones and a distinctive change in the content of siliciclastic material. A distinctive change in the character of the natural gamma radiation record also reflects this major switch. The diminished accumulation of biogenic sediments subsequent to this boundary may reflect an overall environmental degradation, while barren intervals within Unit I may be linked to high-amplitude climatic cycles within the late Pleistocene.

Variations in the nonbiogenic sediment components are as important as the biogenic components in understanding this site. A dramatic change in the composition and texture of terrigenous sediment is evident between the upper two units and lower two units of the record. Upsection increases in quartz, feldspar, and dropstones suggest a link to the onset of increased glaciation during the Pliocene. Changes in natural gamma-ray emissions may be related to a shift in the suite of clay minerals. All of the above could likely be linked to changes associated with (1) erosional rates and style, (2) relative importance of individual source areas, and (3) delivery mechanisms. A possible source for coarse detrital material within Units I and II is indicated by episodic concentrations of sand and gravel (Fig. 8), which may be rare expressions of episodic gravity flows related to eustatic sea-level change.

## BIOSTRATIGRAPHY

Site 907, located on the central Iceland Plateau, and including Holes 907B and 907C, yielded a sedimentary sequence of middle Miocene to Holocene age (~16.0 to 0 Ma). Calcareous nannofossils, planktonic foraminifers, and benthic foraminifers are present down to about 40 mbsf. With the exception of two intervals with rare occurrences of calcareous nannofossils, only siliceous microfossils were

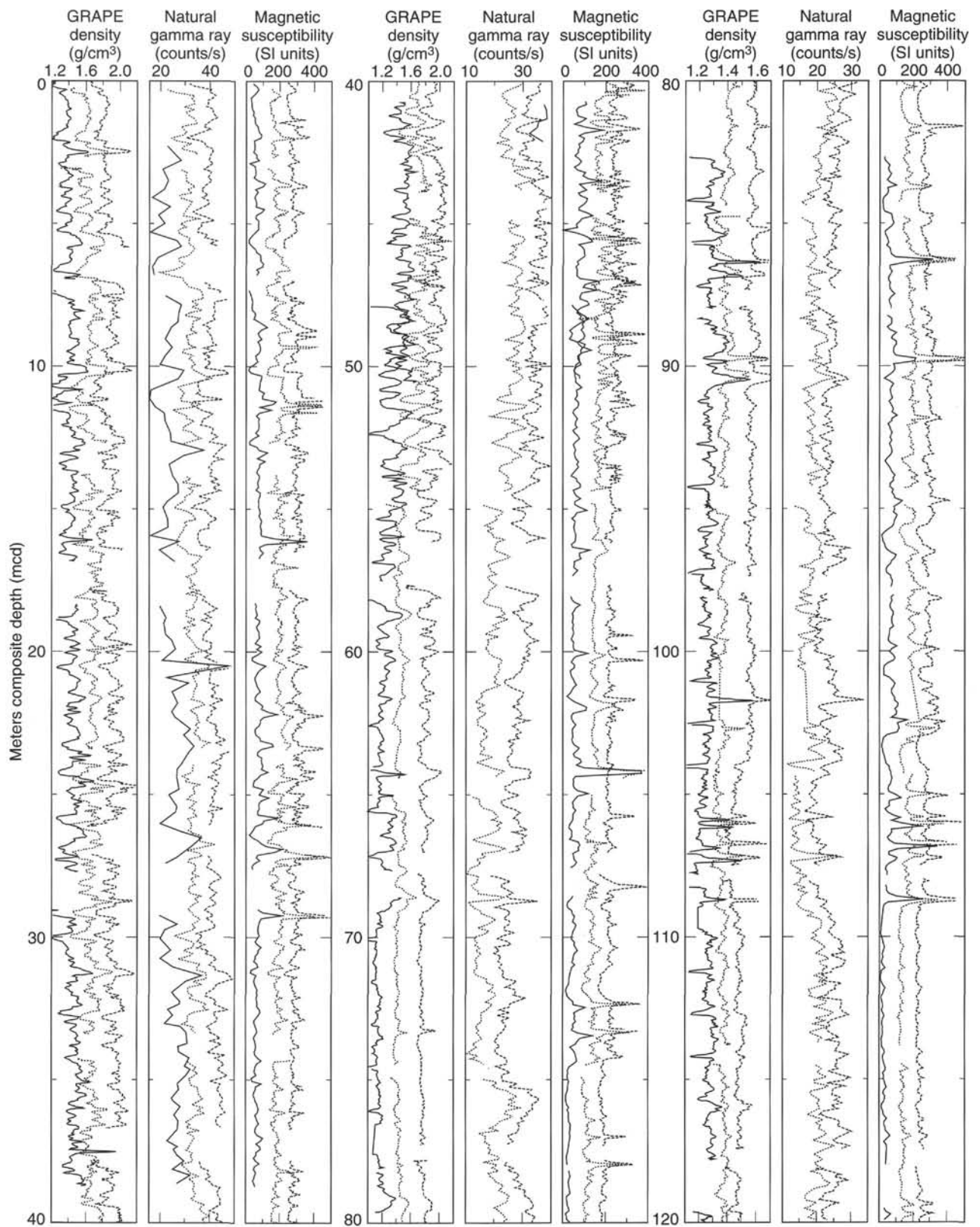


Figure 3. GRAPE density, natural gamma radiation, and magnetic susceptibility data from Site 907 on the mcd (meters composite depth) scale. Lines for Holes 907B (dotted) and 907C (dashed) have been horizontally offset from line for Hole 907A (solid) for better display; therefore, values given on horizontal scale are the true values only for Hole 907A. (See also back pocket.)

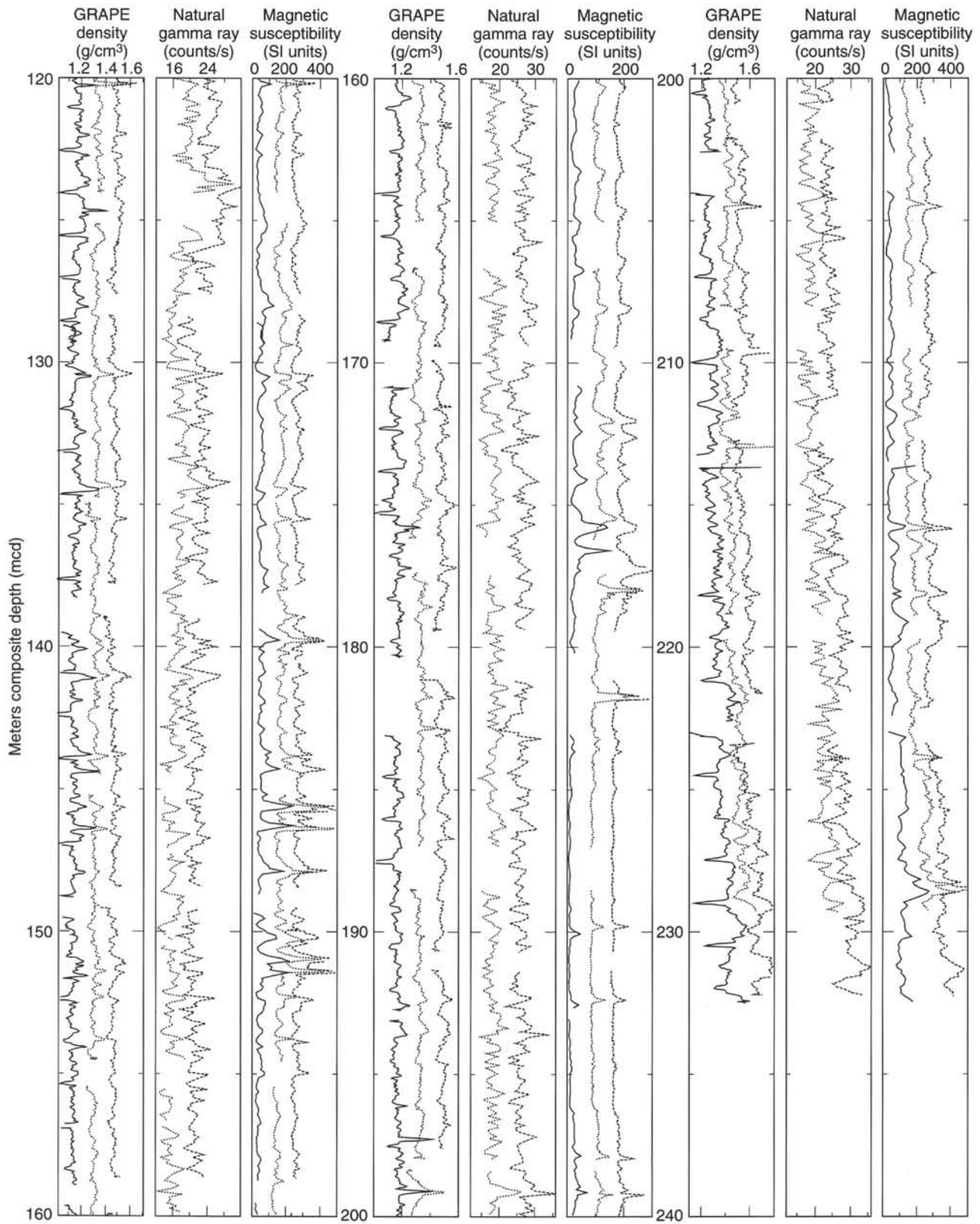


Figure 3 (continued).

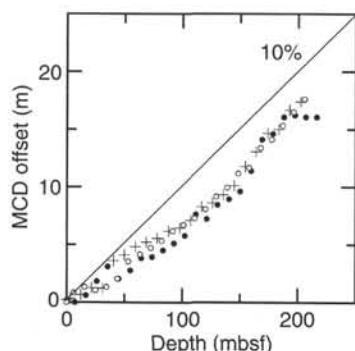


Figure 4. Depth offsets of the Site 907 meters composite depth scale relative to mbsf depth, illustrating the “growth” of the composite depth scale. Solid circles = Hole 907A, crosses = Hole 907B, open circles = Hole 907C.

Table 3. Site 907 splice tie points for “907A” splice.

Hole, core, section (cm)	Depth (mbsf)	Depth (mcd)	Hole, core, section (cm)	Depth (mbsf)	Depth (mcd)
<b>162-907-</b>					
A-1H-4, 128	5.70	5.70	tie to	B-2H-2, 117	5.37
B-2H-3, 118	6.87	7.20	tie to	C-2H-1, 24	6.34
C-2H-1, 134	7.44	8.30	tie to	A-2H-1, 104	8.27
A-2H-4, 149	13.20	13.23	tie to	C-2H-5, 27	12.37
C-2H-5, 146	13.56	14.42	tie to	B-3H-1, 65	12.85
B-3H-4, 32	17.02	18.59	tie to	C-3H-1, 80	16.40
C-3H-2, 68	17.78	19.97	tie to	A-3H-2, 26	18.47
A-3H-6, 149	25.70	27.20	tie to	C-4H-1, 17	25.27
C-4H-2, 87	27.47	29.42	tie to	A-4H-1, 46	26.69
A-4H-6, 146	35.17	37.90	tie to	C-5H-1, 12	34.72
C-5H-3, 70	38.29	41.47	tie to	A-5H-1, 84	36.54
A-5H-5, 86	42.57	47.50	tie to	B-6H-2, 124	43.43
B-6H-4, 138	46.58	50.65	tie to	A-6H-2, 141	48.11
A-6H-7, 59	54.80	57.34	tie to	C-7H-1, 4	53.64
C-7H-3, 95	57.54	61.56	tie to	A-7H-3, 59	58.30
A-7H-7, 38	64.10	67.36	tie to	B-8H-2, 89	62.09
B-8H-3, 89	63.59	68.86	tie to	A-8H-1, 38	64.60
A-8H-5, 42	70.64	74.90	tie to	C-8H-5, 117	70.26
C-8H-7, 17	72.26	76.90	tie to	B-9H-2, 53	71.22
B-9H-3, 56	72.75	78.43	tie to	C-9H-1, 65	73.25
C-9H-3, 77	76.37	81.55	tie to	A-9H-3, 35	71.07
A-9H-6, 95	82.17	86.55	tie to	B-10H-2, 34	80.53
B-10H-3, 88	82.58	88.60	tie to	A-10H-1, 44	83.67
A-10H-6, 14	90.87	95.80	tie to	B-11H-1, 97	89.17
B-11H-3, 102	92.22	98.85	tie to	A-11H-1, 92	93.62
A-11H-7, 7	101.79	107.01	tie to	B-12H-2, 125	100.45
B-12H-5, 82	104.52	111.08	tie to	A-12H-2, 149	105.20
A-12H-6, 135	111.08	116.96	tie to	B-13H-2, 103	109.73
B-13H-4, 110	112.79	120.02	tie to	A-13H-1, 59	112.30
A-13H-6, 148	120.69	128.41	tie to	C-14H-1, 11	120.21
C-14H-2, 31	121.91	130.11	tie to	A-14H-2, 8	122.80
A-14H-6, 119	129.90	137.21	tie to	B-15H-2, 81	128.50
B-15H-4, 98	131.68	140.39	tie to	A-15H-1, 107	131.80
A-15H-6, 28	138.52	147.11	tie to	B-16H-2, 44	137.64
B-16H-5, 57	141.19	150.66	tie to	A-16H-1, 138	141.61
A-16H-6, 78	148.51	157.56	tie to	B-17H-2, 62	147.32
B-17H-4, 48	150.17	160.41	tie to	A-17H-1, 94	150.66
A-17H-6, 145	158.66	168.41	tie to	B-18H-2, 29	156.49
B-18H-3, 136	159.06	170.98	tie to	C-18H-1, 110	159.20
C-18H-3, 121	162.31	174.09	tie to	A-18H-3, 38	162.60
A-18H-6, 61	167.32	178.81	tie to	B-19H-1, 142	165.62
B-19H-4, 19	168.89	182.08	tie to	C-19H-1, 98	168.58
C-19H-2, 103	170.13	183.63	tie to	A-19H-6, 8	169.40
A-19H-7, 28	178.03	192.26	tie to	C-20H-1, 96	178.06
C-20H-3, 61	180.71	194.91	tie to	A-20H-2, 43	180.18
A-20H-6, 118	186.93	201.66	tie to	B-21H-3, 33	186.53
B-21H-3, 122	187.41	202.54	tie to	C-21H-1, 47	187.07
C-21H-3, 54	190.14	205.61	tie to	A-21H-2, 17	189.42
A-21H-6, 147	196.72	212.91	tie to	B-22H-3, 42	196.12
B-22H-5, 8	198.77	215.56	tie to	A-22H-2, 51	199.21
A-22H-6, 75	205.50	221.84	tie to	B-23H-2, 63	204.33
B-23H-4, 146	208.15	225.67	tie to	A-23H-2, 125	209.50
A-26X-2, 86	223.20	239.37			

Table 4. Site 907 splice tie points for “907B/C” splice.

Hole, core, section (cm)	Depth (mbsf)	Depth (mcd)	Hole, core, section (cm)	Depth (mbsf)	Depth (mcd)
<b>162-907-</b>					
C-1H-4, 131	5.80	5.80	tie to	B-2H-2, 128	5.47
B-2H-3, 119	6.88	7.21	tie to	C-2H-1, 25	6.35
C-2H-5, 146	13.56	14.42	tie to	B-3H-1, 65	12.85
B-3H-4, 32	17.02	18.59	tie to	C-3H-1, 80	16.40
C-3H-6, 23	23.33	25.52	tie to	B-4H-2, 17	23.37
B-4H-3, 49	25.19	27.34	tie to	C-4H-1, 29	25.39
C-4H-7, 29	34.38	36.33	tie to	B-5H-2, 56	33.26
B-5H-3, 109	35.29	38.36	tie to	C-5H-1, 58	35.18
C-5H-6, 62	42.72	45.90	tie to	B-6H-1, 113	41.83
B-6H-3, 91	44.61	48.68	tie to	C-6H-2, 59	46.18
C-6H-6, 95	52.54	55.04	tie to	A-6H-5, 128	52.50
A-6H-7, 59	54.80	57.34	tie to	C-7H-1, 4	53.64
C-7H-3, 95	57.54	61.56	tie to	A-7H-3, 59	58.30
A-7H-7, 38	64.10	67.36	tie to	B-8H-2, 89	62.09
B-8H-2, 146	62.66	67.93	tie to	C-8H-1, 19	63.29
C-8H-7, 17	72.26	76.90	tie to	B-9H-2, 53	71.22
B-9H-3, 56	72.75	78.43	tie to	C-9H-1, 65	73.25
C-9H-6, 146	81.56	86.74	tie to	B-10H-2, 52	80.72
B-10H-3, 110	82.79	88.81	tie to	C-10H-1, 95	83.04
C-10H-6, 47	90.06	95.83	tie to	B-11H-1, 101	89.20
B-11H-3, 143	92.63	99.26	tie to	C-11H-1, 136	92.96
C-11H-6, 49	99.59	105.89	tie to	B-12H-2, 14	99.33
B-12H-3, 113	101.83	108.39	tie to	C-12H-1, 46	101.56
C-12H-6, 119	109.78	116.61	tie to	B-13H-2, 68	109.38
B-13H-4, 119	112.88	120.11	tie to	C-13H-2, 59	112.69
C-13H-6, 77	118.86	126.28	tie to	B-14H-1, 119	117.89
B-14H-4, 67	121.87	130.26	tie to	C-14H-2, 46	122.06
C-14H-7, 20	129.30	137.50	tie to	B-15H-2, 109	128.79
B-15H-3, 140	130.60	139.31	tie to	C-15H-1, 41	130.01
C-15H-6, 53	137.63	146.93	tie to	B-16H-2, 26	137.46
B-16H-5, 59	141.21	150.68	tie to	C-16H-2, 5	140.65
C-16H-6, 146	148.06	158.09	tie to	B-17H-2, 116	147.85
B-17H-4, 37	150.07	160.31	tie to	C-17H-1, 44	149.04
C-17H-6, 101	157.11	168.38	tie to	B-18H-2, 26	156.46
B-18H-3, 136	159.06	170.98	tie to	C-18H-1, 110	159.20
C-18H-6, 119	166.79	178.57	tie to	B-19H-1, 119	165.38
B-19H-4, 19	168.89	182.08	tie to	C-19H-1, 98	168.58
C-19H-6, 133	176.43	189.93	tie to	B-20H-1, 146	175.16
B-20H-3, 65	177.35	192.12	tie to	C-20H-1, 82	177.92
C-20H-7, 8	186.18	200.38	tie to	B-21H-2, 56	185.25
B-21H-3, 122	187.41	202.54	tie to	C-21H-1, 47	187.07
C-21H-6, 41	194.51	209.98	tie to	B-22H-1, 49	193.19
B-22H-5, 8	198.77	215.56	tie to	C-22H-2, 134	198.94
C-22H-5, 146	203.56	220.18	tie to	B-23H-1, 47	202.66
B-23H-6, 19	209.89	227.41	tie to	C-23H-3, 107	209.67
C-23H-6, 143	214.53	232.37			

found from about 40 mbsf to the bottom of the section. Hence, diatoms and siliceous flagellates provide the only biostratigraphic information for the deeper part of the hole. Biostratigraphic zones for calcareous nannofossils, planktonic foraminifers, diatoms, and siliceous flagellates are summarized in Figure 10. The biostratigraphic datums displayed in Table 7 are combined with magnetic polarity data to estimate sedimentation rates (see “Sedimentation Rates” section, this chapter).

### Calcareous Nannofossils

All core-catcher samples from Hole 907B were examined for nannofossils. In addition, one sample per core section was examined from Cores 162-907B-1H through 3H. Below this level, selected samples from some suspected carbonate-bearing intervals were also examined. Calcareous nannofossils mainly occur in the first three cores, and their abundances fluctuate considerably. As coccolithophores are photosynthetic and cannot live under a permanent ice cover, intervals with nannofossils can be interpreted as representing open-water conditions (with no perennial ice cover). Intervals without nannofossils in the presence of planktonic foraminifers may be interpreted as periods with perennial ice cover. There are also variations in the amount of reworked Cretaceous nannofossils in the three cores. These Cretaceous nannofossils were ice-rafted from the North Sea area. Their variations may be used to monitor fluctuations in icebergs reaching Site 907 from the North Sea. Quantitative, high-resolution studies of in situ nannofossils, as well as reworked Cretaceous

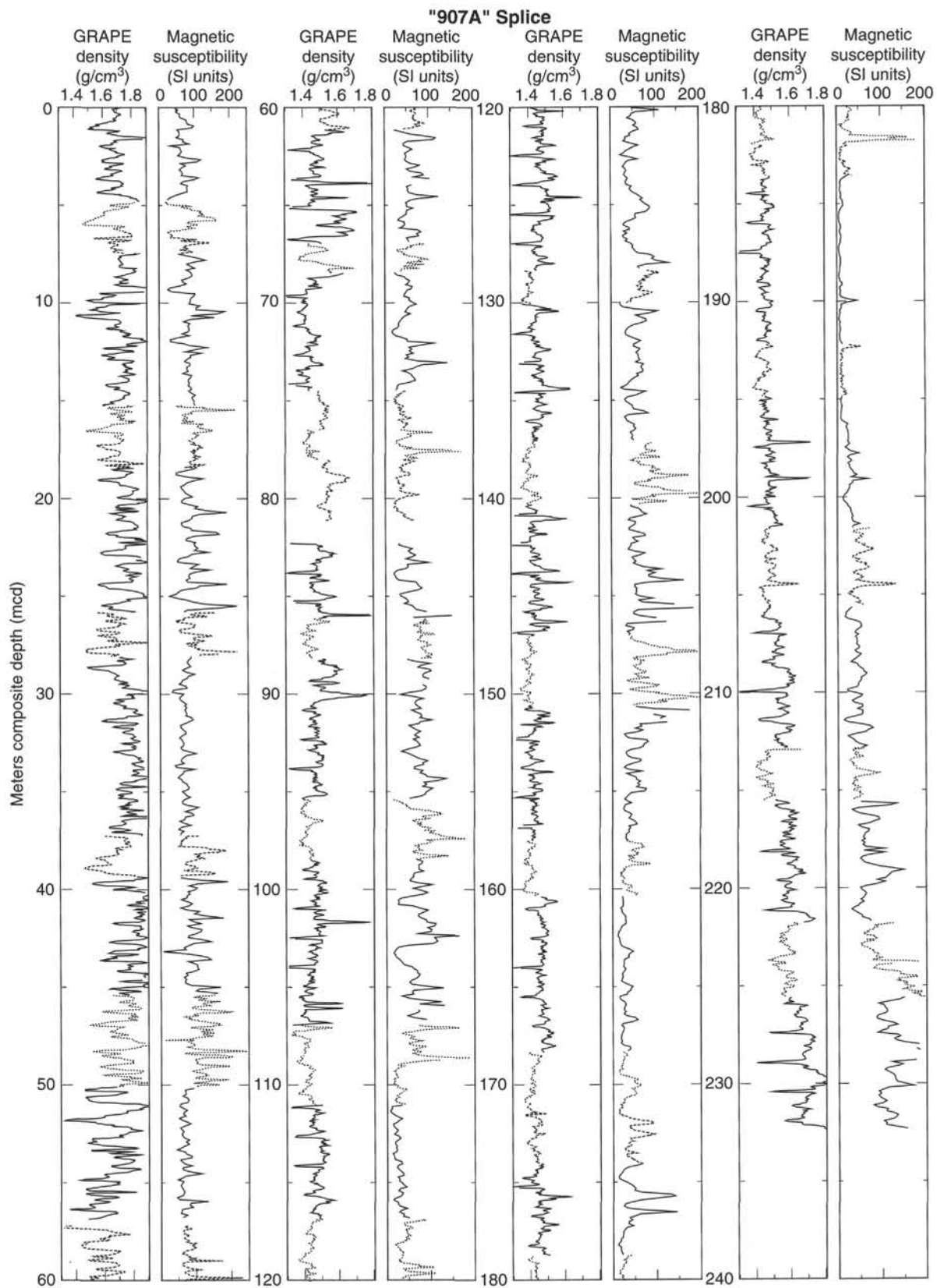


Figure 5. Spliced records of GRAPE density and magnetic susceptibility data from Site 907, using the "907A splice." GRAPE values for Holes 907B and 907C have been increased by 0.28 g/cm<sup>3</sup> to bring mean values in line with Hole 907A GRAPE values (see "Physical Properties" section, this chapter). Tie points for forming the splice are given in Table 3. Holes are 907A (solid), 907B (dotted), and 907C (dashed).

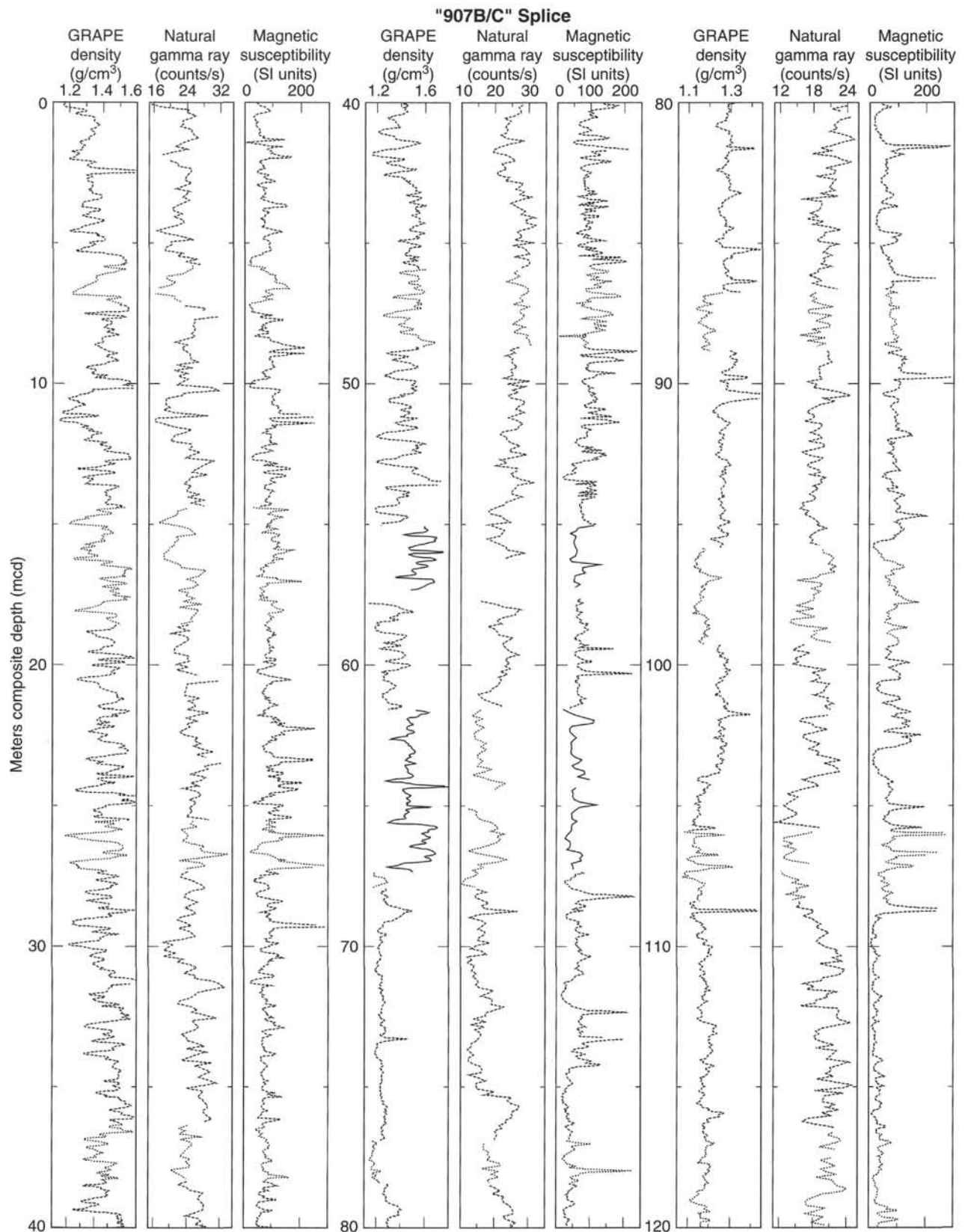


Figure 6. Spliced records of GRAPE density, natural gamma radiation, and magnetic susceptibility data from Site 907, using the "907B/C splice." Tie points for forming the splice are given in Table 4. Holes are 907A (solid), 907B (dotted), and 907C (dashed).

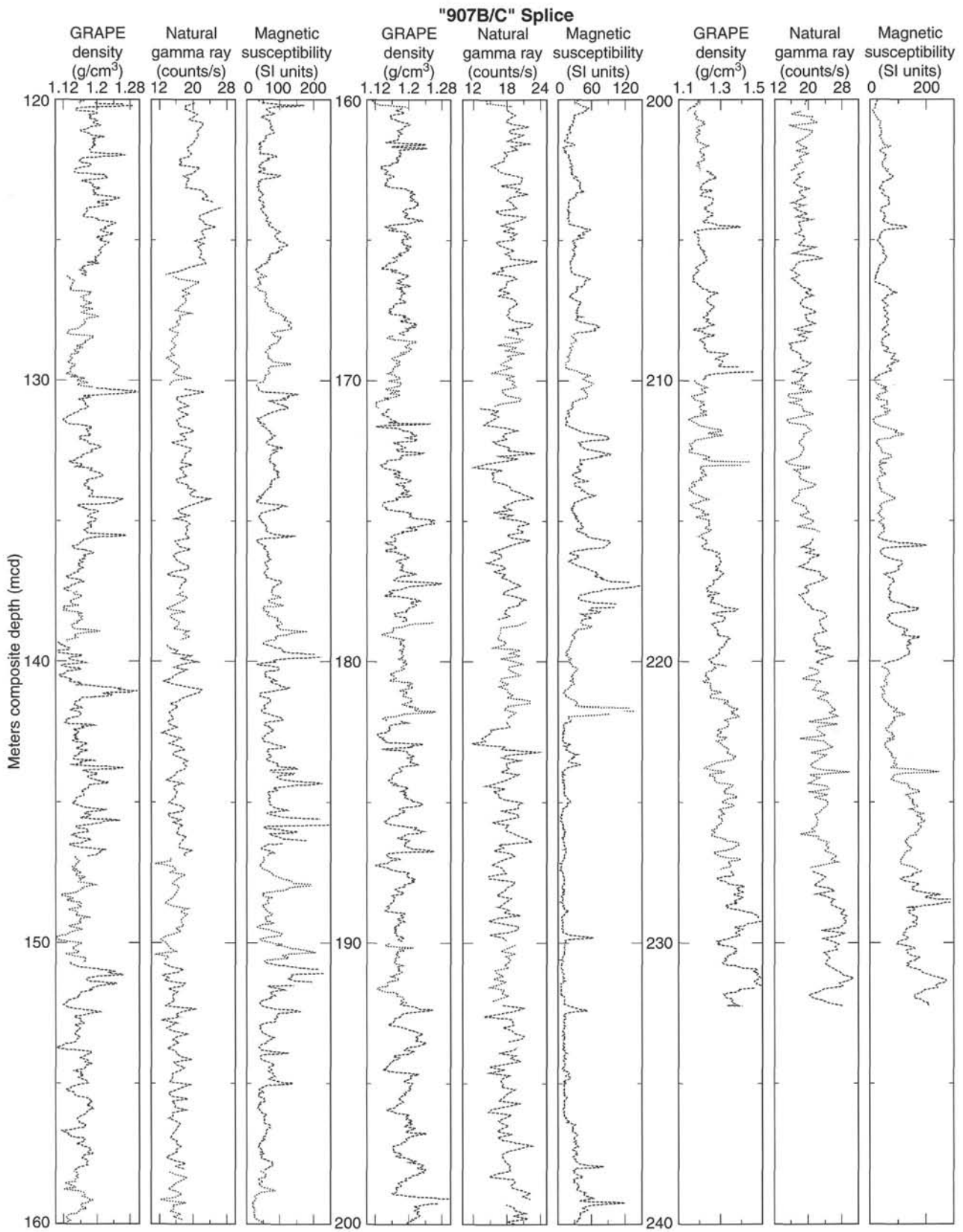


Figure 6 (continued).

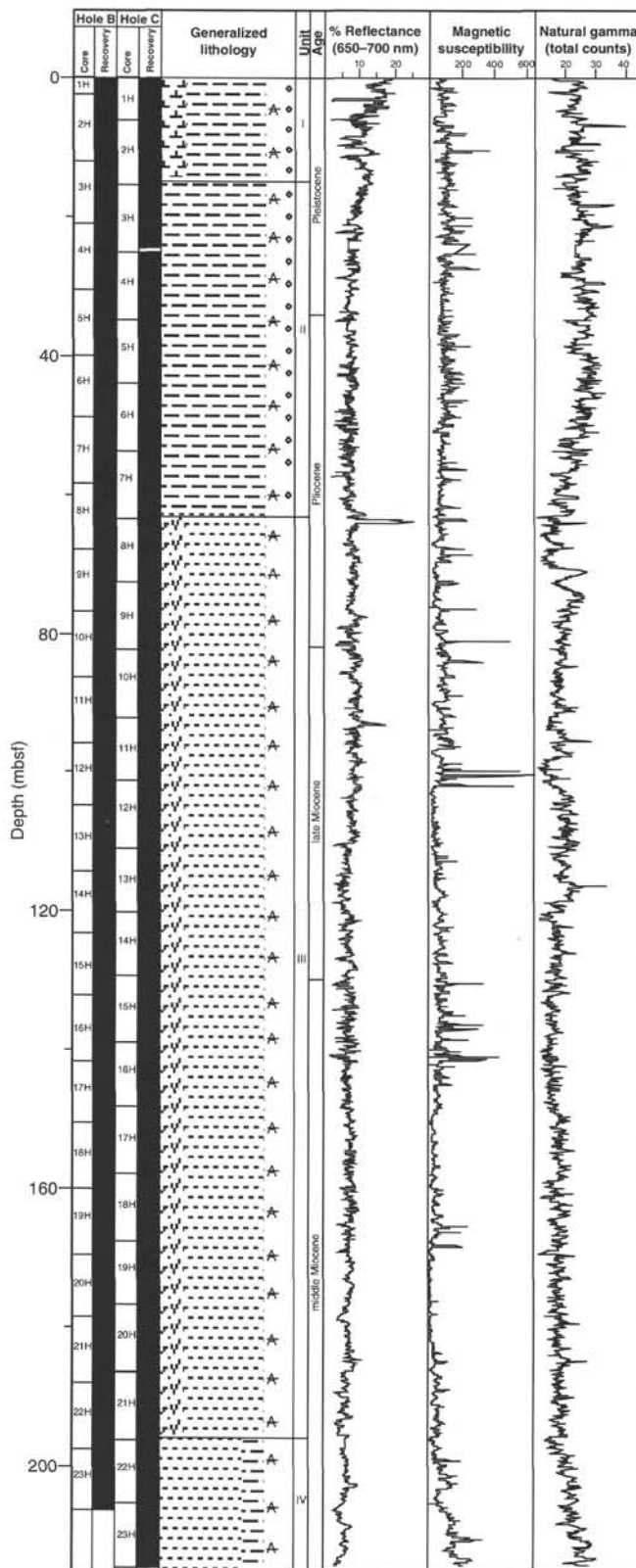


Figure 7. Core recovery, lithostratigraphy, age, percentage reflectance (red band, 650–700 nm), magnetic susceptibility, and natural gamma radiation of sediments recovered in Holes 907B and 907C. (Key to symbols used in the “Generalized Lithology” column can be found in fig. 4, “Explanatory Notes” chapter, this volume.)

Table 5. Summary table of dropstones greater than 1 cm in size found in lithostratigraphic Units I and II at Site 907.

Core, section, interval top (cm)	Depth (mbsf)	Size (cm)	Composition	Shape
<b>162-907B-</b>				
1H-1, 39	0.4	4.8	Oxidized basalt	Subrounded
1H-2, 20	0.2	1.8	Sedimentary	Subrounded
1H-2, 30	0.3	2.5	Oxidized basalt (?)	Subrounded
2H-2, 48	4.7	1.2	Basalt	Subangular
2H-5, 28	8.9	3.4	Basalt	Subangular
3H-1, 110	13.3	3.3	Basalt	Rounded
3H-2, 25	13.9	1.2	Basalt	Rounded
3H-2, 43	14.1	2.5	Dark siltstone (?)	Subangular
3H-6, 80	20.5	1.5	Basalt	Subrounded
3H-6, 10	19.8	2.2	Basalt	Subrounded
4H-1, 68	22.4	2.0	Gneiss	Subrounded
4H-2, 136	23.1	1.0	Diorite	Subrounded
4H-2, 148	23.2	1.0	Scoria	Angular
5H-4, 65	36.4	1.1	Black basalt	Angular
6H-4, 21	44.4	1.3	Gray-black igneous	Angular
6H-4, 119	45.4	1.8	Iron-oxidized layered siltstone	Subrounded
6H-5, 7	45.8	1.6	Gray igneous	Subangular
<b>162-907C-</b>				
1H-1, 116	1.2	1.7	Sedimentary	Angular
1H-1, 143	1.4	2.0	Basalt	Subrounded
2H-1, 21	0.2	1.7	Black siltstone	Subangular
2H-4, 34	10.9	1.3	Gray siltstone	Subangular
2H-4, 132	11.9	2.1	Pink-gray igneous	Subrounded
2H-6, 43	14.0	2.4	Black basalt	Round
3H-3, 45	19.1	3.0	Gabbro	Subrounded
4H-4, 133	30.9	1.4	Basalt	Subrounded
5H-3, 80	38.4	2.2	Basalt	Subround
5H-4, 143	40.5	1.5	Basalt	Round
5H-5, 90	41.5	1.4	Basalt	Subangular
5H-5, 145	42.1	1.2	Basalt	Subangular
6H-2, 60	46.2	3.0	Flintstone	Angular
6H-5, 90	51.0	6.0	Sandstone	Subrounded
6H-5, 100	51.1	1.0	White granite	Round
7H-2, 78	55.9	2.1	Black shale (?)	Subrounded
7H-4, 16	58.3	1.8	Diorite	Subangular
7H-6, 27	62.9	1.1	Pumice	Angular

nannofossils, should provide useful data for reconstructing the history of surface-water thermal gradients and circulation patterns in the Norwegian-Greenland Sea.

Sample 162-907B-1H-1, 0–1 cm, contains common *Coccolithus pelagicus* and rare *Emiliania huxleyi*. Rare specimens of *E. huxleyi* are also present in Sample 162-907B-1H-1, 115 cm. Several samples immediately below this level are either barren of nannofossils or contain rare specimens of nannofossils. This hinders the precise location of the first occurrence of *E. huxleyi*. Only one specimen of *Pseudoemiliania lacunosa* was found in Sample 162-907B-3H-2, 39 cm, and thus the last occurrence datum of this species cannot be meaningfully applied.

Abundant *Coccolithus pelagicus* were found in several light-colored intervals in Core 162-907B-8H. This species is generally known to be the most tolerant of cold waters and among the most dissolution-resistant species. The lowermost occurrence of nannofossils was found in Section 162-907C-11H-2, where nannofossils are strongly fragmented due to dissolution. Some whole specimens of *C. pelagicus* are present and two specimens of *Reticulofenestra pseudumbilicus* are seen. The presence of the latter species suggests an age older than 3.6 Ma (lower Pliocene). This carbonate-bearing interval was not seen in Hole 907B, presumably due to a coring gap in that hole.

### Planktonic Foraminifers

Planktonic foraminifers are found only in the upper part of the sequence; they are common in Samples 162-907B-1H-CC and 2H-CC, and rare in Samples 162-907B-3H-CC and 4H-CC. Assemblages are dominated by *Neoglobobquadrina pachyderma* (sinistrally coiling variety), indicating subpolar/polar paleoenvironmental conditions. The start of the acme zone of *N. pachyderma* (sinistrally coiling) is

Table 6. Summary table of lithostratigraphic units at Site 907.

Unit	Depth (mbsf)	Thickness (m)	Age	Dominant lithologies/criteria
I	0–15.6	15.6	Holocene–“mid.” Pleist.	Biogenic microfossil mixed sediment, silty clay, clay with silt, clay. High-amplitude and decreasing trend of reflectance, high amount of quartz and feldspar, color change between Units I and II.
II	15.6–63.1	47.5	“mid.” Pleist.–“mid.” Plio.	Silty clay, clay with silt and ash, clay. High amount of quartz and feldspar, absence of biogenic sediment, onset of dropstones, downcore increase in natural gamma radiation.
III	63.1–196.1	133.0	“mid.” Plio.–mid. Mio.	Dark greenish gray silty clay, clay with silt, clay with diatoms. Reoccurrence of siliceous sediment, relatively lower amount of siliciclastic material, no trend in magnetic susceptibility and natural gamma radiation.
IV	196.1–214.9	18.8	middle Miocene	Dark greenish gray silty clay, clay with silt and clay. Downcore increase in magnetic susceptibility and natural gamma radiation, no biogenic sediment, slightly lower amount of siliciclastic material.

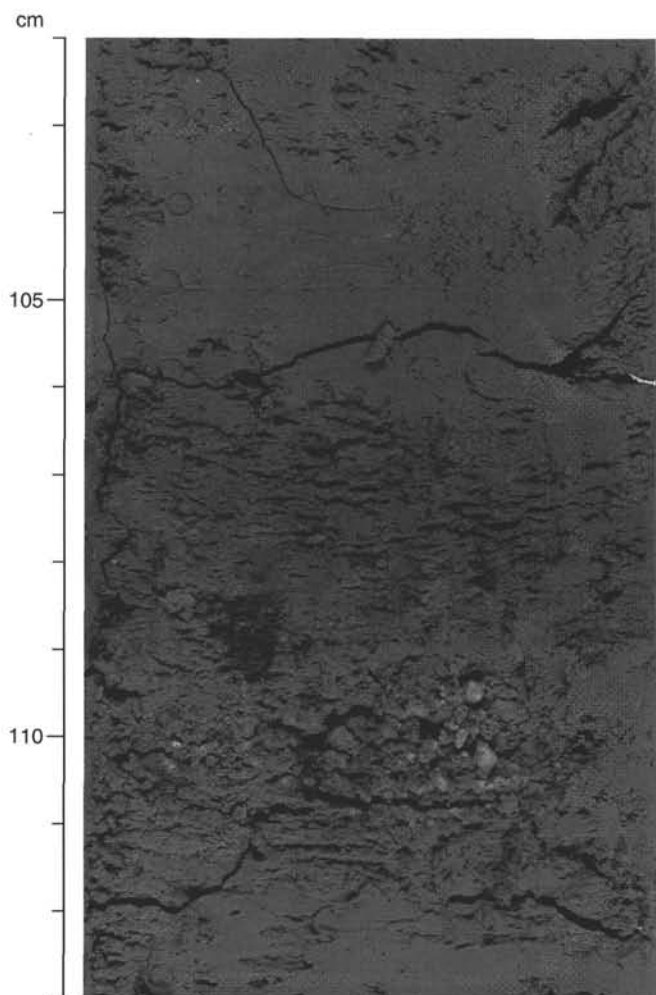


Figure 8. Coarse detrital material found in Section 162-907B-2H-6, 102–113 cm.

not found at this site due to samples barren of planktonic foraminifers (Fig. 10).

### Benthic Foraminifers

Benthic foraminifers are present through the upper part of the sequence, decreasing in abundance and diversity from the mudline (Sample 162-907B-1H, 0–1 cm), where stained specimens of *Cibicides wuellerstorfi* are very abundant, to Sample 162-907B-3H-CC where only rare, broken, and etched specimens occur. Additional

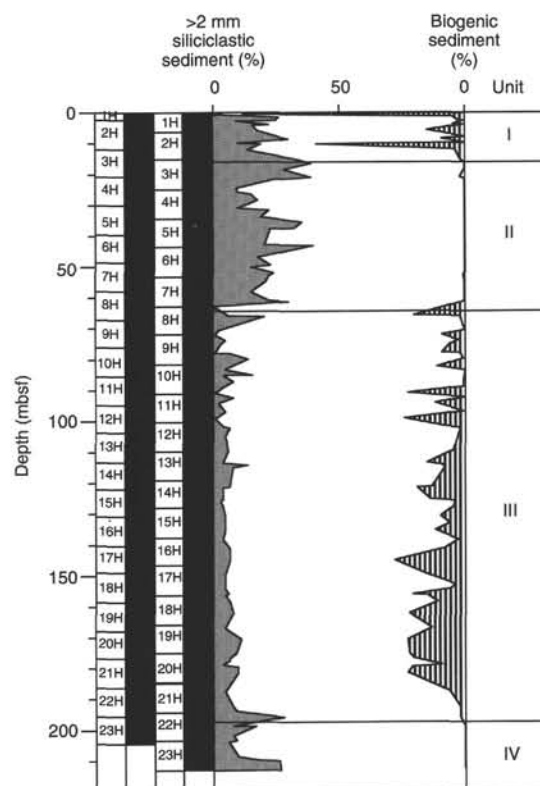


Figure 9. Graphic summary of smear slide data from Holes 907B and 907C. Gray shaded area is &gt;2-mm siliciclastic sediment and hatched area is biogenic sediment.

taxa common to Samples 162-907B-1H-CC and 2H-CC include *Bolivina* spp., *Cassidulina teretis*, *Eponides umbonatus*, and *Pullenia* spp. Rare fragments of the agglutinated foraminifers *Spirosigmoinella* sp. and *Martinottiella communis* occur between Samples 162-907B-15H-CC and 23H-CC, suggesting a middle Miocene age, corresponding to Zone D of Hole 907A (Shipboard Scientific Party, 1995).

### Diatoms

Diatom abundance, preservation, and zonation from Hole 907B is similar to that of Hole 907A. Small differences in the depth of biostratigraphic datums can be accounted for by the offset in mbsf of Holes 907A and 907B.

Diatom abundances at Site 907 vary from barren during the Pleistocene, to abundant during the middle to late Miocene. Samples 162-

Table 7. Depth range of biostratigraphic datums, Site 907.

Datums	Age (Ma)	Core, section, interval (cm)	Depth (mbsf)	Depth (mcd)
		162-907B-		
LO <i>E. cornuta</i> (E)	2.61	8H-2, 124 8H-CC, 21-23	62.44 69.47	67.26 74.29
FO <i>T. zabelinae</i> (D)	3.90	8H-CC, 21-23 10H-4, 39-41	69.47 83.59	74.29 89.16
FO <i>T. oestrupii</i> (D)	5.20	11H-CC, 21-23 13H-1, 39-41	97.91 107.59	104.09 114.71
LO <i>P. bispinum</i> (S)	5.23	10H-CC, 20-22 11H-2, 70	88.50 90.40	94.07 96.58
LO <i>M. diodon</i> (S)	5.93	11H-2, 70 11H-CC, 21-23	90.40 97.91	96.58 104.09
LO <i>P. apiculata</i> (S)	6.59	12H-CC, 21-23 13H-2, 44	107.53 109.14	113.98 116.26
FO <i>S. barboi</i> (D)	9.50	13H-2, 39-41 13H-3, 39-41	109.09 110.59	116.21 117.71
LO <i>D. hustedtii</i> (D)	10.00	12H-CC, 21-23 13H-CC, 22-24	107.53 117.06	113.98 124.18
LO <i>C. depressus</i> (S)	12.39	20H-3, 11 20H-CC, 23-26	176.81 186.97	191.47 201.63

Notes: FO = first occurrence; LO = last occurrence. In parentheses: D = diatom, S = silicoflagellate, and E = ebridian.

907B-1H-CC to 5H-CC, which correspond to the *T. oestrupii* and upper *R. barboi* zones of Schrader and Fenner (1976), are barren of diatoms. Diatoms are present in Samples 162-907B-6H-CC to 10H-CC, representing the lower *R. barboi*, *T. kryophila*, and *C. marginatus* Zones. Abundances during this interval vary from trace to few. During the late Miocene *D. hustedtii*, middle to late Miocene *C. biharensis*, and late Miocene *G. tenue* zones, diatoms are abundant and well preserved. Sample 162-907B-22H-CC is barren.

**Siliceous Flagellates**

Below a barren interval at the top of the section, siliceous flagellates (including silicoflagellates, ebridians, and actiniscidians) are continuously present downsection in Hole 907B. The abundance of these microfossils varies from trace to abundant, the preservation from moderate to poor.

**Silicoflagellates**

Sample 162-907B-1H-1, 10 cm, represents the Pleistocene *Distephanus speculum* Zone. Below, a barren interval follows between Samples 162-907B-1-CC and 6H-CC. Samples 162-907B-8H-2, 124 cm, to 11H-2, 70 cm, are assigned to the Pliocene *Distephanus aculeatus* Zone. Samples 162-907B-11H-CC to 12H-3, 147 cm, are placed in the *Mesocena diodon* Zone, which approximates the Pliocene/Miocene boundary. Samples 162-907B-13H-2, 44 cm, to 20H-3, 11 cm, belong to the *Paramesocena circulus apiculata* Zone. Due to the last occurrence of *Cannopilus depressus*, Samples 162-907B-20H-CC and 21H-CC are attributed to the Upper *Corbisema triacantha* Zone. Samples 162-907B-22H-CC and 23H-CC are barren of silicoflagellates.

**Ebridians and Actiniscidians**

Sample 162-907B-1H-1, 10 cm, belongs into the Pleistocene *Actiniscus pentasterias* Zone. Below, a barren interval follows between Samples 162-907B-1-CC and 6H-CC. Because of nondiagnostic species, Samples 162-907B-7H-CC and 8H-2, 124 cm, remain unzoned. From Sample 162-907B-8-CC to 10H-3, 20 cm, the upper to lower Pliocene *Ebriopsis cornuta* Zone is present. Samples 162-907B-11H-2, 70 cm, to 13H-CC are assigned to the upper Miocene *Parathrani-*

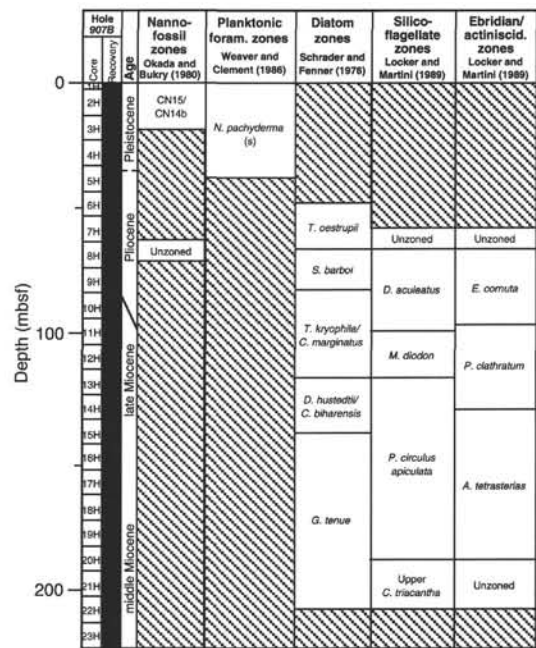


Figure 10. Biostratigraphic summary, Site 907. Hatched intervals indicate absence of fossils. Dashed line at Pliocene/Pleistocene boundary reflects uncertainty in exact placement based on planktonic foraminifer data. Diagonal line separating Miocene/Pliocene indicates inconsistent ages between diatom, silicoflagellate, and ebridian/actiniscid. zones.

*um clathratum* Zone. Between Samples 162-907B-14H-CC and 20H-3, 11 cm, an *Actiniscus tetraasterias* Zone can be determined, which correlates with the *Paramesocena circulus apiculata* Zone of silicoflagellates. The section from Sample 162-907B-20H-CC to 23H-CC includes an unzoned interval above a barren interval.

**PALEOMAGNETISM**

At Site 907, archive halves of all core sections from Holes 907B and 907C were measured using the pass-through cryogenic magnetometer with a 5-cm measurement interval. Demagnetization was carried out at peak alternating fields of 25 mT for all core sections. Additional demagnetization steps at 30 mT were carried out on some core sections, as time allowed (Table 8). The ubiquitous drilling-induced remanence is steeply inclined downward, and therefore mimics a normal-polarity geomagnetic field which may mask reversed-polarity intervals. This magnetic overprint can have relatively high coercivity and is not always fully removed at peak demagnetization fields of 30 mT, the largest demagnetization field available in conjunction with the pass-through cryogenic magnetometer. Due to incomplete removal of the drill-string magnetization, reversed-polarity intervals are often represented by low inclination data and are more poorly defined than normal-polarity intervals (Fig. 11). In addition, the upper 25%-50% of Section 1 of most cores appears particularly susceptible to high coercivity (drill-string) remagnetization, which is not always removed at peak alternating fields of 25 or 30 mT.

At the 25-mT demagnetization level, magnetization intensities lie in the 1-20 mA/m range. The inclination records at Holes 907B and 907C can be correlated without serious difficulty, and these in turn can be correlated to Hole 907A (drilled during Leg 151) (Fig. 11). There are, however, three intervals where we see discrepancies among the inclination records. (1) In the 60-80-mbsf interval, the record of the Gilbert Chron is different for the three holes. The data

**Table 8. Summary of pass-through cryogenic magnetometer measurements from Holes 907B and 907C.**

Measurement	Core sections
25 mT	162-907B-
30 mT	1H-1 through 23H-6
	2H-4, 3H-1 through 3H-5, 4H-1, 8H-1, 8H-5, 9H-2, 9H-3, 9H-6,
	10H-1, 10H-2, 11H-4, 11H-6, 12H-1, 12H-5, 12H-6, 15H-5,
	16H-2, 21H-1, 22H-3, 23H-2, 23H-3
25 mT	162-907C-
30 mT	1H-1 through 23H-6
	2H-6, 2H-7, 3H-1, 3H-3, 3H-4, 5H-3, 5H-5, 6H-1, 8H-3, 9H-5,
	11H-1, 11H-4, 11H-5, 15H-1, 15H-2, 15H-5, 15H-6, 16H-1, 17H-1,
	20H-6, 21H-1, 23H-5

are particularly noisy in this interval, possibly due to remagnetization carried by authigenic iron sulfides. (2) The apparent Gauss/Matuyama boundary occurs at 47.85 mbsf in Hole 907B, at 53.25 mbsf in Hole 907C, and at 49.00 mbsf in Hole 907A (Fig. 11). There is no obvious explanation for these differences. The cores from these intervals are not visibly deformed. The inclination record from Holes 907A and 907B appear to have higher fidelity in this interval. (3) In the basal 30 m, 185–205 mbsf, the inclination records are inconsistent, with the record at Hole 907A being particularly inconsistent with those from Holes 907B and 907C.

The Brunhes/Matuyama boundary and the Jaramillo and Olduvai Subchrons are well defined and identifiable in all three holes at Site 907 (Table 9). Below the Matuyama Chron, the correlation of polarity chrons to the geomagnetic polarity time scale (GPTS) is problematic. There is no obvious pattern fit of polarity zones to the GPTS.

On Leg 151 the predominantly normal polarity zones in the intervals 110–130 mbsf and 160–180 mbsf were correlated to Chron 5n.2 and Chron 5ABn/5ACn, respectively (Myhre, Thiede, Firth, et al., 1995) (Fig. 11). We consider it more likely that the 110–130-mbsf interval correlates to Chron 4n.2 and that the 160–180-mbsf interval correlates to Chron 5ACn/5ADn (Fig. 11). This modification of the Leg 151 interpretation, named Interpretation 2 in Figures 11 and 12, is based partly on the different inclination record which we obtained in the basal 20 m of this recovered section. We adopt this revised correlation as the most plausible interpretation, and note that this correlation implies changes in sedimentation rate (Fig. 12) for which there is no apparent biostratigraphic or sedimentological evidence. However, it is interesting to note that four intervals of high bulk density and low water content occur at 63, 100, 132, and 184 mbsf in Hole 907B (see “Physical Properties” section, this chapter). These levels coincide with the intervals in which changes in sedimentation rate are implied by the revised magnetostratigraphic interpretation (Fig. 12).

This alternative interpretation for the Miocene part of the section seems warranted. In this interpretation, the normal-polarity zone in the 100–130-mbsf interval is correlated to Chron 4n (Fig. 11). The mixed-polarity zone in the 130–140-mbsf interval is correlated to Chron 4r. The 140–160-mbsf interval becomes Chron 4A, and the 160–180-mbsf interval is then Chron 5n.1n/5n.2n. This interpretation may be preferable, as it does not imply large hiatuses in the record, although changes in sedimentation rate are required (Fig. 12).

The magnetostratigraphic interpretation prior to the Gauss/Matuyama boundary remains uncertain. The resolution of the biostratigraphy at this site is insufficient to adequately constrain the interpretations. Shore-based analysis of discrete samples should improve the polarity stratigraphy and may resolve the uncertainties in the correlation of polarity zones to the GPTS.

## SEDIMENTATION RATES

A sedimentary section 216 m thick was recovered at Site 907, extending from the Miocene to the Holocene. Sedimentation rate recon-

**Table 9. Preliminary positions of polarity chron boundaries at Holes 907B and 907C.**

Core, section, interval (cm)	Depth (mbsf)	Interpreted boundary	Age (Ma)	Comments
162-907B-				
3H-1, 110	13.30	Brunhes/Matuyama	0.78	
3H-4, 40	17.10	Jaramillo (top)	0.99	
3H-5, 30	18.50	Jaramillo (bottom)	1.07	
5H-3, 30	34.50	Olduvai (top)	1.77	
5H-5, 130	38.50	Olduvai (bottom)	1.95	
5H-7, 40	40.60	Reunion (top)	2.14	
6H-1, 90	41.60	Reunion (bottom)	2.15	
6H-5, 115	47.85	Matuyama/Gauss	2.58	
8H-7, 10	68.80	Cochiti (top)	4.18	
9H-2, 50	71.20	Cochiti (bottom)	4.29	
9H-3, 105	73.25	Nunivak (top)	4.48	
9H-4, 15	73.85	Nunivak (bottom)	4.62	
9H-4, 120	74.90	Sidufjall (top)	4.80	
9H-6, 70	77.40	Sidufjall (bottom)	4.89	
9H-7, 35	78.55	Thvera (top)	4.98	
10H-2, 0	80.20	Thvera (bottom)	5.23	Section break
11H-1, 15	88.35	Gilbert/C3An	5.89	
12H-6, 95	106.15	(2) C3Bn/C3Br	7.09	
13H-3, 70	110.90	(1) C5n.1r/C5n.2n	9.92	
		(2) C3Br.3r/C4n.1n	7.43	
15H-2, 45	128.15	(1) C5n.2n/C5r.1r	10.95	
		(2) C4n.2n/C4r.1r	8.07	
16H-4, 30	140.50	(1) C5Aar/C5ABn	13.30	
		(2) C4r/C4An	8.70	
17H-1, 115	146.35	(1) C5ABn/C5Abr	13.51	
		(2) C4An/C4Ar	9.02	
18H-5, 15	160.85	(1) C5ABr/C5ACn	13.70	
		(2) C4Ar.3r/C5n.1n	9.74	
19H-1, 110	165.30	(1) C5ACn/C5ACr	14.08	
		(2) C5n.1n/C5n.1r	9.88	
19H-3, 30	167.50	(1) C5ACr/C5ADn	14.18	
		(2) C5n.1r/C5n.2n	9.92	
20H-6, 10	181.30	(1) C5ADn/C5ADr	14.61	
		(2) C5n.2n/C5r.1r	10.95	
162-907C-				
21H-6, 40	14.00	Brunhes/Matuyama	0.78	
3H-1, 130	18.40	Jaramillo (bottom)	1.07	
5H-1, 0	34.80	Olduvai (top)	1.77	Core break
5H-3, 35	37.95	Olduvai (bottom)	1.95	
6H-7, 15	53.25	Matuyama/Gauss	2.58	
10H-5, 55	88.65	Gilbert/C3An	5.89	
12H-4, 45	106.05	(2) C3Bn/C3Br	7.09	
13H-1	110.70	(1) C5n.1r/C5n.2n	9.92	Core break
		(2) C3Br.3r/C4n.1n	7.43	
14H-6, .	128.65	(1) C5n.2n/C5r.1r	10.95	
		(2) C4n.2n/C4r.1r	8.07	
16H-2, 0	140.60	(1) C5Aar/C5ABn	13.30	Section break
		(2) C4r/C4An	8.70	
16H-5, 140	146.55	(1) C5ABn/C5Abr	13.51	
		(2) C4An/C4Ar	9.02	
18H-2, 125	160.85	(1) C5ABr/C5ACn	13.70	
		(2) C4Ar.3r/C5n.1n	9.74	
18H-6, 105	166.65	(1) C5ACn/C5ACr	14.08	
		(2) C5n.1n/C5n.1r	9.88	
19H-1, 0	167.70	(1) C5ACr/C5ADn	14.18	Core break
		(2) C5n.1r/C5n.2n	9.92	
20H-4, 50	182.10	(1) C5ADn/C5ADr	14.62	
		(2) C5n.2n/C5r.1r	10.95	

Notes: For the Miocene, two alternative interpretations are given. The interpretation labeled (1) is close to that adopted at Hole 907A (Leg 151).

structions for Site 907 were based on magnetic polarity events from all holes (see “Paleomagnetism” section, this chapter). Owing to low abundances of calcareous fossils in the section, combined with uncertain calibrations of siliceous fossils, biostratigraphic events were not used for sedimentation rate estimates (see “Biostratigraphy” section, this chapter). The Site 907 composite depth section (see “Composite Depths” section, this chapter) was used to relate events recorded in Holes 907A, 907B, and 907C to a common depth scale.

Sedimentation rates were calculated for both the meters below seafloor (mbsf) depth scale and the meters composite (mcd) scale. Below the Gilbert/C3An boundary (5.83 Ma, 94.63 mcd), two interpretations of the paleomagnetic record at Site 907 are possible. According to the interpretation of the record from Hole 907A, drilled on Leg 151 (Myhre, Thiede, Firth, et al., 1995), and as discussed further in the “Paleomagnetism” section (this chapter), hiatuses or intervals

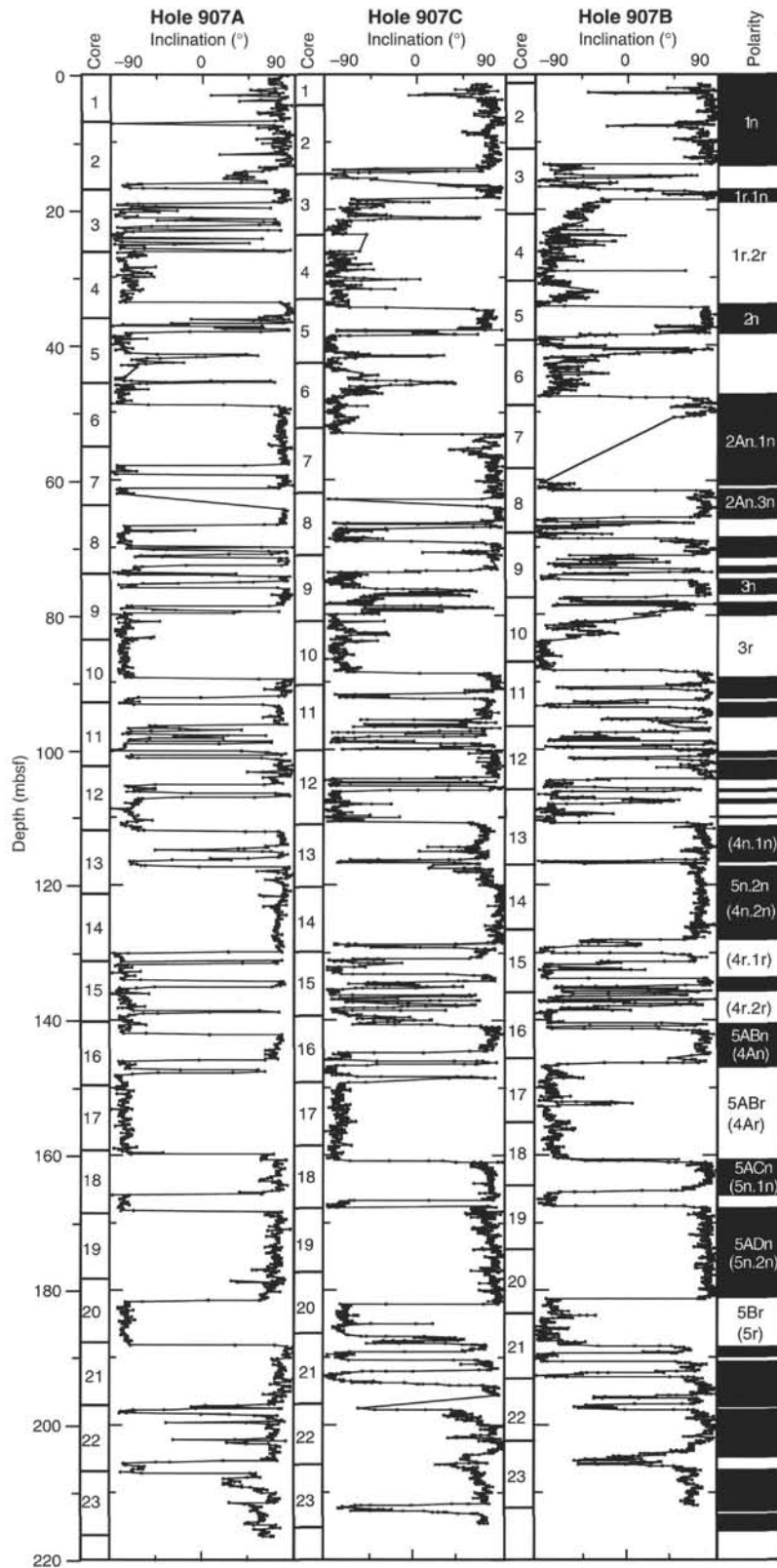


Figure 11. Inclination of the magnetization vector vs. depth (mbsf) after AF demagnetization at a peak field of 30 mT for Hole 907A (Leg 151), and after AF demagnetization at 25 mT for Holes 907B and 907C. For the Miocene, Interpretation 1 (Leg 151) polarity chron assignments are without parentheses; Interpretation 2 (Leg 162) assignments are in parentheses.

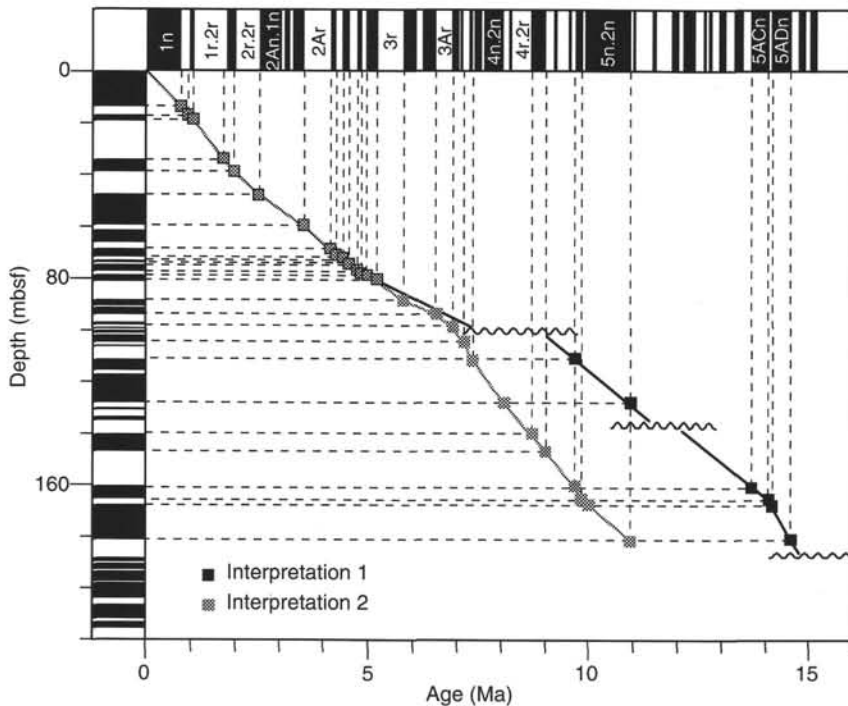


Figure 12. Correlation of Holes 907B and 907C to the geomagnetic polarity time scale (Cande and Kent, 1995). Interpretation 1 is slightly modified after the Hole 907A (Leg 151) interpretation. Interpretation 2 is radically different but does not imply large hiatuses. Wavy lines correspond to levels of high density from physical properties data (see text). The levels of high density correspond to some intervals in which the sedimentation rate is changing, which is implied by the magnetostratigraphic interpretations.

of condensed sedimentation may have occurred at approximately 60 mbsf (between the top of Gauss Chron and the top of the Cochiti Subchron), 100 mbsf (between the top of C3An and the top of C5n.2n), and 130 mbsf (between the top of C5r.1r and the top of C5ABr). However, the sedimentation rates presented here were calculated using the alternate Leg 162 interpretation (see "Paleomagnetism" section, this chapter) which incorporates the records for Holes 907B and 907C and does not invoke major hiatuses.

Average sedimentation rates for Site 907 were determined according to the Leg 162 interpretation, by assuming uniform sedimentation rates between clearly identifiable magnetic events, which are listed in Table 10. Figure 13 presents sedimentation rates as a function of age and composite depth. Because of the discrepancy between the two paleomagnetic interpretations, the average sedimentation rates given in Table 10 and Figure 14 over the intervals discussed above must be regarded as preliminary.

## ORGANIC GEOCHEMISTRY

The shipboard organic geochemistry program at Site 907 consisted of analyses of volatile hydrocarbons, determinations of inorganic carbon, total nitrogen, total carbon, total sulfur, and pyrolysis measurements (for methods, see "Explanatory Notes" chapter, this volume).

### Volatile Hydrocarbon

As part of the shipboard safety and pollution monitoring program, concentrations of methane ( $C_1$ ) and ethane ( $C_2$ ) gases were measured in every core using standard ODP headspace-sampling technique. As in Hole 907A, cored during ODP Leg 151, the methane content remained very low throughout the sediment sequence in Hole 907B (2–3 ppm; Table 11; Fig. 15). Ethane was not detected.

### Carbon, Nitrogen, and Sulfur Concentration

Determinations of inorganic carbon, total carbon, total nitrogen, and total sulfur in Hole 907B are summarized in Table 12 and dis-

played in Figure 15. According to the carbonate content data, the sediment sequence of Hole 907B can be divided into two intervals (Fig. 15). The upper interval (0–15 mbsf; Holocene to late Pleistocene) of Hole 907B, which corresponds to lithostratigraphic Unit I (see "Lithostratigraphy" section, this chapter), is characterized by high amplitude variations of carbonate percentages ranging from 1.0% to 55.5% (Fig. 15). In the lower interval (15–209.2 mbsf) of Hole 907B, the carbonate content is nearly zero throughout, except for three distinct increases in  $CaCO_3$  content, in Samples 162-907B-6H-1, 83–84 cm, 8H-2, 124–125 cm, and 11H-3, 70–71 cm, with values of 43.8%, 64.8%, and 26.2%, respectively (Fig. 15; Table 12).

Total organic carbon (TOC) contents vary between 0.04% and 1.66%, with an average value of 0.49% (Fig. 15; Table 12). Low values of <0.5% are dominant in the interval between 0 and 171 mbsf, where the mean TOC is 0.31%. However, the average TOC content in the lowermost interval (171–209.2 mbsf; middle Miocene), at 0.77%, is considerably higher than in the upper interval. This middle Miocene enrichment of organic carbon in the sediments may reflect increased surface-water productivity at that time. Total nitrogen contents are generally very low (0.03%–0.37%; Table 12). Total sulfur values range from 0% to 3.24%, with an average of 0.60% (Fig. 15; Table 12), and higher values in the lower section of Hole 907B (128.9–209.2 mbsf; late to middle Miocene). This sulfur is probably pyritic sulfur given the occurrence of significant amounts of pyrite nodules in the lowermost interval (see "Lithostratigraphy" section, this chapter).

An organic carbon vs. sulfur diagram provides information about the depositional environment (Stein, 1990; Fig. 16). As stated above, sulfur is mainly found as pyritic sulfur in siliciclastic marine sediments. Sulfur is available in excess as sulfate in seawater, thus the limiting factor for pyrite formation under normal oxic seawater conditions is the amount of organic matter (which controls the formation of reducing conditions in the near-surface sediments). In this environment, there is a positive correlation between sulfur and organic carbon (e.g., Berner, 1984). Under anoxic seawater conditions,  $H_2S$  exists in the seawater. Thus, framboidal pyrite is initially formed in the water column, resulting in a surplus of sulfur in the organic carbon vs. sulfur diagram (Leventhal, 1983). In oxic and high-productivity conditions, the sediments are thus characterized by high

Table 10. Age control points, Site 907.

Event	Age (Ma)	907A (mbsf)	907A (mcd)	907B (mbsf)	907B (mcd)	907C (mbsf)	907C (mcd)	Avg. depth (mbsf)	Avg. depth (mcd)	Rate (mbsf/m.y.)	Rate (mcd/m.y.)
Core top	0.00	0.00	0.00	0.00	0.00	0.00	0.00	0.00	0.00	18.57	19.62
Brunhes/Matuyama	0.78	16.15	16.18	13.30	14.87	14.00	14.86	14.48	15.30	12.34	15.75
Jaramillo top	0.99	17.05	18.55	17.10	18.67			17.08	18.61	20.10	22.83
Jaramillo bottom	1.07	19.15	20.65	18.50	20.07	18.40	20.59	18.68	20.44	22.43	23.61
Olduvai top	1.77	33.85	36.58	34.50	37.57	34.80	36.75	34.38	36.97	21.90	27.56
Olduvai bottom	1.95	38.15	43.08	38.50	41.57	37.95	41.13	38.33	41.93	14.47	16.58
Reunion II top	2.14	41.55	46.48	40.60	43.67			41.08	45.08	20.39	18.20
Matuyama/Gauss	2.58	49.05	51.59	47.85	51.92	53.25	55.75	50.05	53.09	12.08	13.16
Cochiti top	4.18	69.95	74.21	68.80	74.07			69.38	74.14	16.36	18.23
Cochiti bottom	4.29	71.15	75.41	71.20	76.88			71.18	76.15	6.71	6.71
Nunivak top	4.48	71.65	75.91	73.25	78.93			72.45	77.42	6.07	6.07
Nunivak bottom	4.62	72.75	77.01	73.85	79.53			73.30	78.27	7.08	7.42
Sidufjall top	4.80	74.25	78.63	74.90	80.58			74.58	79.61	20.00	20.00
Sidufjall bottom	4.89	75.35	79.73	77.40	83.08			76.38	81.41	10.28	10.28
Thvera top	4.98	76.05	80.43	78.55	84.23			77.30	82.33	8.72	9.38
Thvera bottom	5.23	78.75	83.13	80.20	86.22			79.48	84.68	14.21	14.77
Gilbert/C3An	5.89	89.55	94.48	88.35	94.37	88.65	94.42	88.85	94.42	14.38	15.14
C3Bn/C3Br	7.09			106.15	112.71	106.05	112.48	106.10	112.60	13.82	15.40
C3Br.3r/C4n.1n	7.43			110.90	118.13	110.70	117.53	110.80	117.83	27.50	29.73
C4n.2n/C4r.1r	8.07	105.25	111.13	128.15	136.86	128.65	136.85	128.40	136.86	19.29	21.34
C4r/C4An	8.70	111.85	117.73	140.50	149.97	140.60	150.63	140.55	150.30	18.44	19.64
C4An/C4Ar	9.02	114.55	122.27	146.35	156.59	146.55	156.58	146.45	156.59	20.00	22.38
C4Ar.3r/C5n.1n	9.74			160.85	172.77	160.85	172.63	160.85	172.70	36.61	41.14
C5n.1n/C5n.1r	9.88			165.30	178.49	166.65	178.43	165.98	178.46	40.63	40.63
C5n.1r/C5n.2n	9.92	117.05	124.77	167.50	180.69	167.70	179.48	167.60	180.09	13.69	15.63
C5n.2n/C5r.1r	10.95	129.75	137.06	181.30	196.07	182.10	196.30	181.70	196.19		

Notes: Ages are from Berggren et al. (1995). Depths from Hole 907A below the Gilbert/C3An boundary are not included in the average depths or calculated sedimentation rates.

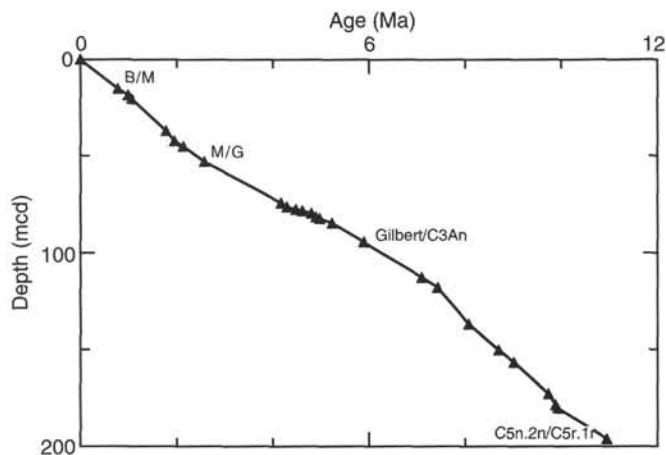


Figure 13. Site 907 age vs. depth (mcd) curve based on the interpretation given in the "Paleomagnetism" section (this chapter). B/M = Brunhes/Matuyama; M/G = Matuyama/Gauss.

organic carbon and high sulfur content, and in anoxic conditions, they are characterized by a surplus of sulfur. On the other hand, sediments of open-ocean low productivity conditions are characterized by very low sulfur and organic carbon contents (Stein, 1990). Figure 16 is a diagram of TOC vs. TS from Hole 907B. The data set derived from the upper interval (0–171 mbsf) in Hole 907B appears to reflect a low-productivity interval, whereas sediments from the lowermost interval (171–209.2 mbsf) indicate an enrichment of sulfur in the middle Miocene. These data suggest that the environment of deposition was more anoxic due to increased productivity and/or restricted deep-water ventilation during the middle Miocene.

#### Composition of Organic Matter

C/N ratios vary between 0.2 and 14.1 (Fig. 15; Table 12). These data suggest a predominance of marine organic material, probably with a mixture between marine and terrigenous organic carbon in the lowermost interval where the mean C/N ratio is 10.6 (Fig. 17). Most of the Rock-Eval pyrograms show an indistinct bimodal  $S_2$  peak in Hole 907B. Pyrograms of immature sediments typically show poorly separated  $S_1$  and  $S_2$  peaks, which can give anomalous  $S_2$ ,  $T_{max}$ , HI,

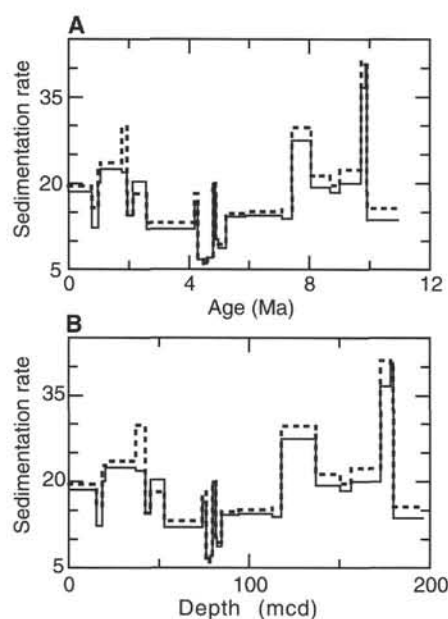


Figure 14. **A.** Average Site 907 sedimentation rates vs. age, based on magnetostratigraphic events listed in Table 10. **B.** Site 907 sedimentation rates vs. composite depth. Solid lines indicate rates in mbsf/m.y.; dashed lines indicate rates in mcd/m.y.

and OI values (Peters, 1986). Therefore, these results suggest the occurrence of an immature type of organic matter.

#### Flux of Organic Carbon

Organic carbon concentrations are transformed into mass accumulation rate, following van Andel et al. (1975):

$$\text{MARTOC} = \text{TOC}/100 \times \text{LSR} \times \text{DD},$$

where MARTOC is mass accumulation rate of total organic carbon ( $\text{g}/\text{cm}^2/\text{k.y.}$ ), LSR is linear sedimentation rate ( $\text{cm}/\text{k.y.}$ ; from "Sedimentation Rates" section, this chapter), and DD is dry density ( $\text{g}/\text{cm}^3$ ; from "Physical Properties" section, this chapter). The average mass accumulation rates of total organic carbon are low, varying between 0.001 and 0.012  $\text{g}/\text{cm}^2/\text{k.y.}$  in Hole 907B (Fig. 18; Table 13). Very low values occur in the interval between late middle Miocene and late Pliocene (15–2.6 Ma). MARTOC values are relatively higher in the interval from late Pliocene to Pleistocene; however, these values are similar to those observed in modern open-ocean, low-productivity environments (0.001–0.007  $\text{g}/\text{cm}^2/\text{k.y.}$ ; e.g., Stein, 1991). In the middle Miocene section, the accumulation rate of total organic carbon increased to 0.014  $\text{g}/\text{cm}^2/\text{k.y.}$  These data indicate that surface-water productivity and/or preservation of

Table 11. Results of headspace gas analysis of Hole 907B samples.

Core, section, interval (cm)	Depth (mbsf)	C <sub>1</sub> (ppm)
160-907B-		
1H-2, 0-5	1.53	2
2H-5, 0-5	8.73	2
3H-5, 0-5	18.23	2
4H-5, 0-5	27.73	2
5H-5, 0-5	37.23	3
6H-5, 0-5	46.73	3
7H-5, 0-5	56.23	3
8H-5, 0-5	65.73	3
9H-5, 0-5	75.23	3
10H-5, 0-5	84.73	3
11H-5, 0-5	94.23	3
12H-5, 0-5	103.73	3
13H-5, 0-5	113.23	3
14H-5, 0-5	122.73	3
15H-5, 0-5	132.23	3
16H-5, 0-5	140.65	3
17H-5, 0-5	151.23	2
18H-5, 0-5	160.73	2
19H-5, 0-5	170.23	3
20H-5, 0-5	179.73	3
21H-5, 0-5	189.23	3
22H-5, 0-5	198.73	3
23H-5, 0-5	208.23	3

Note: C<sub>1</sub> = methane

organic matter increased at that time. However, further qualitative and quantitative organic geochemical data, such as detailed records of flux rates of terrigenous and marine organic carbon, as well as biomarker data, are required before a detailed paleoceanographic interpretation of the organic carbon data can be made.

## INORGANIC GEOCHEMISTRY

### Interstitial Water

Nine interstitial pore-water samples were collected from Hole 907B for comparison with geochemical data collected previously in Hole 907A by ODP Leg 151 (Myhre, Thiede, Firth, et al., 1995). Sulfate concentrations at the top of Hole 907B are near seawater values (27 mM) and decrease to about 23 mM within the upper 50 m (Fig. 19A; Table 14), indicating sulfate reduction. We observed a pronounced difference in sulfate profiles between Hole 907A, where a maximum occurs at 119.25 mbsf, and Hole 907B, which has only a slight increase at 119 mbsf. It is difficult to explain how such large lateral concentration gradients could develop over short distances (Hole 907B is less than 100 m from Hole 907A) or over a two-year period (time since drilling Hole 907A). The Leg 151 Shipboard Scientific Party (1995) speculated that the sulfate peak at 119.25 mbsf in Hole 907A may signify an unexplained supply of sulfate, perhaps associated with the high geothermal gradients measured in the hole (120.7°C/km). Alternatively, the sulfate values in either hole may be erroneous, although the differences appear to be too large to be attrib-

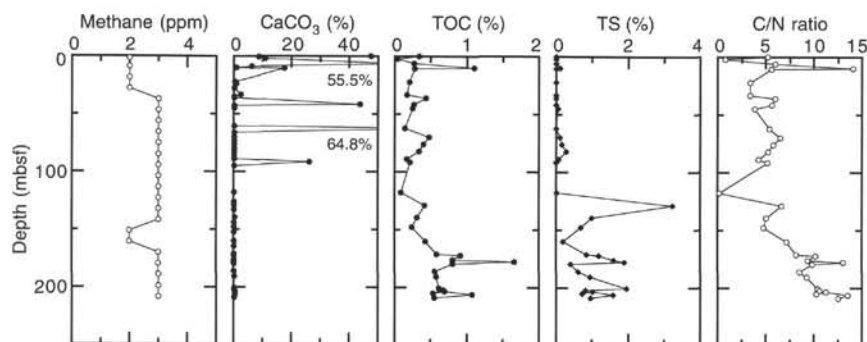


Figure 15. Methane concentration, calcium carbonate ( $\text{CaCO}_3$ ), total organic carbon (TOC), and total sulfur (TS) contents, and TOC/TN (C/N) ratio in Hole 907B.

Table 12. Summary of organic geochemical analyses at Hole 907B samples.

Core, section, interval (cm)	Depth (mbsf)	IC (%)	CaCO <sub>3</sub> (%)	TC (%)	TOC (%)	TN (%)	TS (%)	C/N	C/S
160-907B-									
1H-1, 11-12	0.11	5.72	47.6	6.06	0.34	0.07	0.00	5.2	
1H-1, 66-67	0.66	1.04	8.7						
1H-2, 91-92	2.41	1.30	10.8	1.34	0.04	0.05	0.00	0.8	
2H-3, 70-71	6.40	6.66	55.5	6.93	0.27	0.04	0.00	6.0	
2H-5, 32-33	9.02	0.75	6.2						
2H-5, 125-126	9.95	0.12	1.0	1.22	1.10	0.08	0.11	14.1	9.8
2H-6, 62-63	10.82	2.11	17.6	2.39	0.28	0.05	0.00	5.6	
4H-1, 61-62	22.31	0.06	0.5	0.26	0.20	0.06	0.00	3.4	
4H-2, 64-65	23.84	0.12	1.0						
4H-5, 13-14	27.83	0.04	0.3						
5H-2, 52-53	33.22	0.29	2.4	0.46	0.17	0.05	0.00	3.4	
5H-3, 68-69	34.88	0.03	0.2						
5H-4, 46-47	36.16	0.03	0.2	0.47	0.44	0.07	0.00	6.0	
6H-1, 83-84	41.53	5.26	43.8	5.53	0.27	0.05	0.00	5.7	
6H-2, 62-63	42.82	0.03	0.2						
6H-3, 111-112	44.81	0.03	0.2	0.28	0.25	0.06	0.05	3.9	4.6
8H-1, 76-77	60.46	0.04	0.3						
8H-2, 124-125	62.44	7.78	64.8	7.92	0.14	0.03	0.00	5.4	
8H-5, 49-50	66.19	0.04	0.3						
9H-1, 95-96	70.15	0.03	0.2	0.51	0.48	0.07	0.10	6.5	4.8
9H-3, 95-96	73.15	0.03	0.2						
9H-5, 95-96	76.15	0.03	0.2	0.43	0.40	0.07	0.17	5.8	2.4
10H-1, 63-64	79.33	0.03	0.2						
10H-3, 77-78	82.47	0.03	0.2	0.37	0.34	0.06	0.29	5.3	1.2
10H-5, 75-76	85.45	0.03	0.2						
11H-1, 70-71	88.90	0.03	0.2	0.20	0.17	0.04	0.08	4.3	2.2
11H-3, 70-71	91.90	3.15	26.2	3.36	0.21	0.04	0.00	5.2	
11H-5, 70-71	94.90	0.04	0.3						
14H-1, 102-103	117.72	0.03	0.2	0.12	0.09	0.37	0.02	0.2	4.0
14H-7, 51-52	126.21	0.03	0.2						
15H-2, 116-117	128.86	0.03	0.2	0.45	0.42	0.06	3.24	6.7	0.1
15H-5, 85-86	133.05	0.02	0.2						
16H-3, 73-74	139.43	0.05	0.4	0.36	0.31	0.06	0.99	5.1	0.3
16H-6, 60-61	142.72	0.03	0.2						
17H-2, 104-105	147.74	0.04	0.3	0.28	0.24	0.05	0.69	4.8	0.3
17H-5, 87-88	152.07	0.03	0.2						
18H-4, 74-75	159.94	0.04	0.3	0.47	0.43	0.06	0.19	7.2	2.2
19H-1, 41-42	164.61	0.03	0.2						
19H-5, 103-104	171.23	0.03	0.2	0.62	0.59	0.07	0.86	8.2	0.7
19H-6, 82-83	172.52	0.03	0.2	0.95	0.92	0.09	1.19	10.2	0.8
20H-2, 118-119	176.38	0.04	0.3	0.85	0.81	0.09	1.61	9.4	0.5
20H-3, 138-139	178.08	0.04	0.3	1.70	1.66	0.13	1.90	13.1	0.9
20H-4, 109-110	179.29	0.03	0.2	0.84	0.81	0.08	0.40	9.9	2.1
21H-2, 118-119	185.88	0.04	0.3	0.60	0.56	0.07	0.63	8.5	0.9
21H-5, 113-114	190.33	0.04	0.3	0.62	0.58	0.06	0.95	9.3	0.6
22H-2, 115-116	200.35	0.03	0.2	0.64	0.61	0.06	1.96	10.4	0.3
22H-3, 127-128	201.97	0.04	0.3	0.72	0.68	0.06	0.82	10.6	0.8
22H-5, 117-118	204.87	0.05	0.4	0.58	0.53	0.05	0.74	10.3	0.7
23H-1, 118-119	203.38	0.05	0.4	0.74	0.69	0.06	1.02	11.3	0.7
23H-3, 85-86	206.05	0.05	0.4	1.13	1.08	0.08	1.59	13.5	0.7
23H-5, 103-104	209.23	0.03	0.2	0.58	0.55	0.04	0.96	12.5	0.6
Average:		0.70	5.8	1.47	0.49	0.07	0.60	7.3	1.8
Maximum:		7.78	64.8	7.92	1.66	0.37	3.24	14.1	9.8
Minimum:		0.02	0.2	0.12	0.04	0.03	0.00	0.2	0.1
0-171 m:					0.31		0.3	5.3	
>171 m:					0.77		1.1	10.6	

Notes: IC = inorganic carbon, CaCO<sub>3</sub> = calcium carbonate, TC = total carbon, TOC = total organic carbon, TN = total nitrogen, TS = total sulfur, C/N = total organic carbon/total nitrogen ratios, and C/S = total organic carbon/total sulfur ratios.

uted to analytical error. We remeasured Sample 162-907B-12H-4, 145-150 cm, and obtained nearly the same result. Shore-based work will focus on trying to replicate the high sulfate values observed in archive samples from Hole 907A.

Ammonia concentrations are distinctly greater in Hole 907B than in Hole 907A, although the shapes of the profiles are similar (Fig. 19B). In Hole 907B, ammonia concentrations increase from zero at the surface to a maximum of 211  $\mu\text{M}$  at about 80 mbsf and then decrease to the base of the hole (Fig. 19B; Table 14). An alternative explanation of the observed differences in sulfate and ammonia between Holes 907A and 907B may be that sulfate reduction has been more extensive in Hole 907B, resulting in lowered dissolved sulfate and higher ammonia concentrations. The small decrease in sulfate values of less than 3 mM in Hole 907B is not commensurate with evidence of ubiquitous pyrite in the sediments (see "Lithostratigraphy" section, this chapter). Ash layers in Hole 907B are intensely pyritized, perhaps because the ash serves a source of iron

which reacts with hydrogen sulfide, produced by sulfate reduction, to form iron sulfides (e.g., pyrite).

Unlike the differences in sulfate and ammonia between Holes 907A and 907B, the alkalinity profiles are quite similar and decrease downcore from 3.3 mM at the top to 1.1 mM at the bottom of Hole 907B (Fig. 19C; Table 14). The alkalinity maximum usually associated with sulfate reduction is conspicuously absent at Site 907, and decreasing alkalinity is probably related to steady uptake by alteration of basaltic basement below. Phosphate was measured only in Hole 907B and shows a maximum of 10.6  $\mu\text{M}$  at 13 mbsf followed by decreasing values downcore with low values between 3 and 4  $\mu\text{M}$  below 50 mbsf (Fig. 19D; Table 14).

Calcium concentrations increase and magnesium concentrations decrease downcore in both Holes 907A and 907B (Fig. 19E; Table 14), reflecting diffusional gradients between overlying seawater and seawater-basalt reactions occurring within basement below. The calcium vs. magnesium relationship is linear, which indicates conserva-

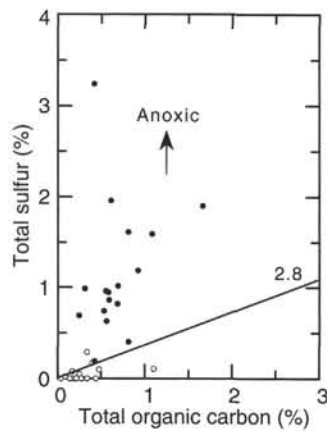


Figure 16. Total organic carbon vs. total sulfur from Hole 907B. Open circles indicate the upper interval (0–171 mbsf) and solid circles indicate the lower-most high-TOC-interval depth range. Line shows C/S ratio of 2.8, the average of normal marine detrital sediments from the Quaternary.

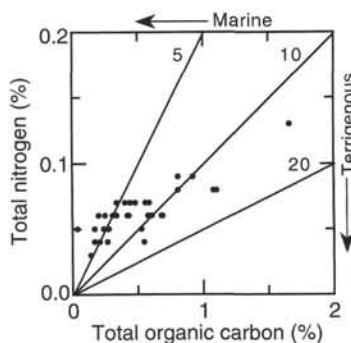


Figure 17. Total organic carbon vs. total nitrogen in Hole 907B. Lines show C/N ratios of 5, 10, and 20.

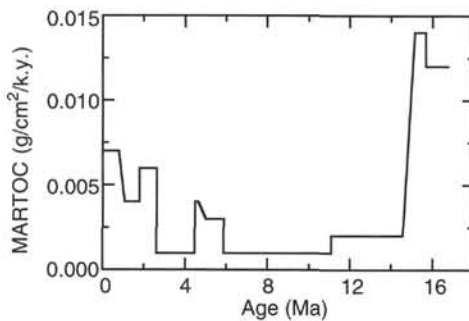


Figure 18. Mass accumulation rate of total organic carbon in Hole 907B.

tive chemical behavior in the sediment column. The  $\Delta\text{Ca}/\Delta\text{Mg}$  slope is  $-1.2$  to  $-1.3$  (Fig. 19F), which is typical for sites on basaltic crust (McDuff, 1981). Potassium concentrations decrease downhole in both Holes 907A and 907B from 12 to 13 mM at the top to values as low as 7 mM at the base of the hole (Fig. 19G; Table 14). The linear trend suggests a diffusive profile with uptake of potassium during alteration of volcanic material within the sediments and by interaction with oceanic crust below.

In both Holes 907A and 907B, silica concentrations increase downhole from about 200  $\mu\text{M}$  at the surface to over 1000  $\mu\text{M}$  in the

Table 13. Average mass accumulation rate of total organic carbon (MARTOC) for different time intervals at Hole 907B.

Age (Ma)	Depth (mbsf)	Avg. TOC (%)	LSR (cm/k.y.)	Dry density (g/cm <sup>3</sup> )	MARTOC (g/cm <sup>2</sup> /k.y.)
0.00	0.00	0.41	1.75	0.92	0.007
0.78	13.30		1.64	0.94	
0.99	17.10		1.75	1.01	
1.07	18.50				
1.77	34.50	0.19	2.31	0.98	0.004
1.95	38.50	0.44	1.99	0.67	0.006
2.14	40.60		1.25	0.91	
2.60	47.85	0.27	2.16	1.02	0.006
2.60	47.85	0.14	0.97	0.69	0.001
4.48	68.80	0.48	1.71	0.47	0.004
4.62	71.20		1.28	0.58	
4.78	73.25		0.60	0.78	
4.88	73.85		0.88	0.64	
5.00	74.90	0.40	1.09	0.64	0.003
5.23	77.40	0.34	1.71	0.58	0.003
5.88	88.35	0.19	0.56	0.57	0.001
9.87	110.90	0.09	1.44	0.51	0.001
11.09	128.15	0.35	0.94	0.50	0.002
14.55	160.85		1.09	0.52	
15.02	165.30		1.25	0.54	
15.15	167.50	0.96	2.66	0.54	0.014
15.68	181.30	0.66	2.66	0.69	0.012

Notes: Linear sedimentation rates (LSR) are based on paleomagnetic stratigraphy and biostratigraphy (see "Sedimentation Rates" section, this chapter). Average dry density values are taken from the "Physical Properties" section (this chapter).

bottom of Hole 907B (Fig. 19H; Table 14). The increase in silica concentrations reflect the dissolution of siliceous microfossils and alteration of volcanic ash in the sediment. In Hole 907A, the deepest sample shows a marked decline in dissolved silica concentrations, but this occurs beyond the depth penetrated by Hole 907B.

Sodium concentrations increase slightly in the top 23 m to maximum of 482 mM and then decrease to minimum values of 467 at the base of Hole 907B (Fig. 19I; Table 14). Chloride concentrations increase downcore from 556 mM at the surface to a maximum of 572 mM near the base of the hole (Fig. 19J; Table 14). The ratio of Na to Cl decreases linearly downhole (Fig. 19K). The increase in chloride may indicate hydration reactions during the alteration of volcanic material to clay; however, this process would also cause sodium to increase. The observed decrease in sodium is probably related to uptake during alteration of volcanic material to form smectite and Na-rich zeolites.

Lithium displays anomalous behavior in that it decreases rapidly downcore from 0 to 25 mbsf and then shows a broad maximum between 50 and 110 mbsf, and then decreases toward the bottom of Hole 907B (Fig. 19L; Table 14). The changes in concentration are small and the complex profile of lithium must indicate sources and sinks in the sediment that may be related to the alteration of abundant volcanic ash in the sediment (see "Lithostratigraphy" section, this chapter). A small increase in strontium concentrations is observed downhole (Fig. 19M; Table 14), which most likely reflects release of strontium from dissolution of calcite.

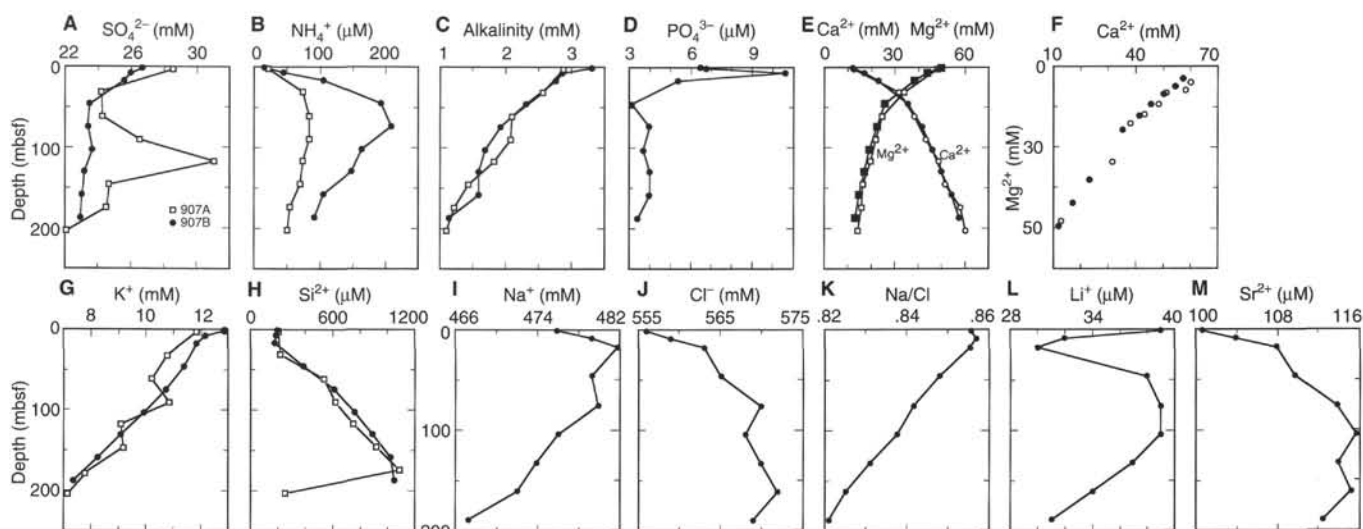


Figure 19. Vertical profiles of sulfate (A), ammonium (B), alkalinity (C), phosphate (D), calcium and magnesium (E), calcium vs. magnesium (F), potassium (G), silica (H), sodium (I), chloride (J), Na/Cl (K), lithium (L), and strontium (M) in Holes 907A (open symbols) and 907B (closed symbols).

Table 14. Composition of interstitial waters in Hole 907B.

Core, section, interval (cm)	Depth (mbsf)	Na (mM)	K (mM)	Li (μM)	Mg (mM)	Ca (mM)	Sr (μM)	Cl (mM)	SO <sub>4</sub> (mM)	NH <sub>4</sub> (μM)	Si (μM)	PO <sub>4</sub> (μM)	pH	Alkalinity (mM)	Salinity
162-907B-															
1H-1, 145-150	4.45	476	12.9	39.0	50.7	11.8	101	556	26.7	15	201	6.5	7.63	3.322	35.0
2H-4, 145-150	13.35	479	12.2	32.0	44.3	16.9	104	559	26.0	45	193	10.6	7.73	2.869	35.0
3H-4, 145-150	22.85	482	11.9	30.0	38.5	23.1	108	563	25.6	107	182	5.4	7.73	2.778	35.5
6H-4, 145-150	51.35	479	11.4	38.0	26.1	35.6	110	565	23.5	194	390	3.2	7.58	2.314	35.5
9H-4, 145-150	79.85	480	10.7	39.0	22.4	41.7	114	570	23.4	211	617	4.0	7.83	1.927	36.0
12H-4, 145-150	108.35	476	9.9	39.0	19.5	46.0	116	568	23.7	166	760	3.7	7.56	1.695	35.5
15H-4, 145-150	136.85	474	9.1	37.0	17.1	50.4	114	570	23.2	150	894	4.0	7.68	1.586	35.5
18H-4, 145-150	165.35	472	8.2	34.0	15.0	54.7	115	572	23.1	107	1033	4.0	7.58	1.598	35.0
21H-4, 145-150	193.85	467	7.3	31.0	13.1	57.6	112	569	23.0	92	1054	3.4	7.63	1.143	35.0

Table 15. Index properties of samples from Hole 907B.

Core, section, interval (cm)	Depth (mbsf)	Water content	Bulk density	Grain density	Dry density	Porosity	Void ratio
		(wet %)	Method C (g/cm <sup>3</sup> )	Method C (g/cm <sup>3</sup> )	Method C (g/cm <sup>3</sup> )	Method C (%)	Method C
162-907B-							
1H-1, 12-14	0.12	59.8	1.36	2.68	0.55	79.6	3.90
1H-1, 27-29	0.27	42.3	1.61	2.78	0.93	66.6	1.99
1H-1, 64-66	0.64	40.5	1.63	2.75	0.97	64.6	1.82
1H-1, 117-119	1.17	40.8	1.64	2.79	0.97	65.2	1.88
1H-2, 10-12	1.60	46.6	1.54	2.73	0.82	69.9	2.32
1H-2, 66-68	2.16	43.4	1.59	2.74	0.90	67.2	2.05
1H-2, 92-94	2.42	45.9	1.57	2.88	0.85	70.5	2.39
2H-1, 32-34	3.02	38.9	1.68	2.82	1.03	63.7	1.75
2H-1, 61-63	3.31	52.6	1.44	2.62	0.68	74.0	2.84

Only part of this table is reproduced here. The entire table appears on the CD-ROM (back pocket).

In summary, good agreement exists for interstitial water chemistry between Holes 907A and 907B for elements that are controlled by chemical alteration and diffusion from oceanic basement (i.e., Ca, Mg, K., Si, and alkalinity). Large discrepancies are observed for biogenic elements involved in sulfate reduction (SO<sub>4</sub><sup>2-</sup> and NH<sub>4</sub>), perhaps reflecting significant lateral or temporal heterogeneity in the bacterially mediated reactions of sulfate reduction.

### PHYSICAL PROPERTIES

The shipboard physical properties program at Site 907 included nondestructive, near-continuous measurements of bulk density, bulk magnetic susceptibility, compressional wave (P-wave) velocity, and natural gamma radiation on whole-round sections of all cores from

**Table 16. Compressional-wave velocity measurements from Hole 907B.**

Core, section, interval (cm)	Depth (mbsf)	Velocity (m/s)	Temperature (°C)	Direction
162-907B-				
1H-1, 13	0.13	1555	21.0	z
1H-1, 29	0.29	1553	20.8	z
1H-1, 65	0.65	1539	20.7	z
1H-1, 119	1.19	1542	20.6	z
1H-2, 9	1.59	1535	20.5	z
1H-2, 67	2.17	1556	20.3	z
1H-2, 92	2.42	1556	20.4	z
2H-1, 31	3.01	1535	20.6	z
2H-1, 120	3.90	1541	20.1	z

Only part of this table is reproduced here. The entire table appears on the CD-ROM (back pocket).

**Table 17. Undrained shear strength measurements from Hole 907B.**

Core, section, interval (cm)	Depth (mbsf)	Undrained shear strength (kPa)	Spring no.	Penetrometer (kPa)
162-907B-				
1H-1, 28	0.28	10.4	1	
1H-1, 120	1.20	11.3	1	
1H-2, 10	1.60	30.9	1	
1H-2, 67	2.17	6.4	1	
1H-2, 92	2.42	28.9	1	
2H-1, 32	3.02	30.8	1	
2H-1, 121	3.91	8.4	1	
2H-2, 14	4.34	30.5	1	
2H-2, 119	5.39	22.4	1	

Only part of this table is reproduced here. The entire table appears on the CD-ROM (back pocket).

**Table 18. Thermal conductivity measurements from Hole 907B.**

Core, section, interval (cm)	Depth (mbsf)	Thermal conductivity (W/(m-K))	Standard error (W/(m-K))
162-907B-			
1H-1, 100	1.00	1.1345	0.00238
1H-2, 100	2.50	1.1987	0.00218
2H-1, 75	3.45	1.1806	0.00322
2H-3, 75	6.45	0.9689	0.00424
2H-5, 75	9.45	1.0306	0.00365
2H-7, 35	12.05	1.0445	0.00354
3H-1, 75	12.95	1.1301	0.00258
3H-3, 75	15.95	1.1337	0.00437
3H-5, 75	18.95	0.9594	0.00299

Only part of this table is reproduced here. The entire table appears on the CD-ROM (back pocket).

each hole using the multisensor track (MST) (See "Explanatory Notes" section, this volume).

Index property measurements (gravimetric density and water content) were made on one to five samples per working half section in all cores (Table 15) (see "Explanatory Notes" chapter, this volume). All discrete measurements were made on samples from Hole 907B. Discrete compressional velocity and undrained vane-shear-strength measurements were made at a resolution of about two to three measurements per working half section (Tables 16, 17). The sonic transducers T1 (z-direction) of the digital sound velocimeter (DSV) were used to a depth of about 10 mbsf; below this depth the use of the DSV was discontinued due to the disruption of the sediment by the acoustic probes (i.e., cracking was observed), and the Hamilton

Frame velocimeter (T3, x-direction) was used to make sonic measurements through the core liner. Thermal conductivity measurements were also made in Hole 907B on three to four whole-round sections per core (Table 18) using the needle probes.

The results from Hole 907B are compared with the results from Hole 907A, which was cored during Leg 151 (see Myhre, Thiede, Firth, et al., 1995, "Site 907" chapter, "Physical Properties" section, p. 86–101).

### Geotechnical Stratigraphy

An evaluation of downhole trends described in this section were used to construct a series of geotechnical units in Hole 907B (Fig. 20). The mean values for index properties, velocity, and shear strength within each of the four geotechnical units are given in Table 19. The offsets between GRAPE density and gravimetric density values are also given in Table 19 for each unit. This offset, which ranged from approximately 0.22 in geotechnical Units G1, G2, and G4, to 0.18 g/cm<sup>3</sup> in Unit G3, is discussed in the "Explanatory Notes" chapter (this volume).

During Leg 151, four geotechnical units were also identified in Hole 907A (Fig. 21; see Myhre, Thiede, Firth, et al., 1995, "Site 907" chapter, "Physical Properties" section, p. 86–101); these same units are maintained for Hole 907B with slight modifications. The boundaries of the geotechnical units and subunits in Hole 907B are given as a specific depth. However, some of these boundaries are more likely defined by a range of sub-bottom depths, so the reasons for their exact placement are discussed.

In Hole 907B, geotechnical Unit G1 extends from the mudline to about 47 mbsf (in Hole 907A, Unit G1 = 0–45 mbsf), which is a zone of variable lithology (e.g., silty clay and clayey silt, with carbonate present in the upper few cores). Unit G1 is defined by generally high bulk density and low porosity values relative to the deeper units. The lower boundary of Unit G1 is most clearly seen in the natural gamma radiation record in Hole 907B (Fig. 20), which is similar in character to the GRAPE density record from Hole 907A (Fig. 21); the GRAPE record in Hole 907B is considered unreliable within this interval due to core disturbance. This boundary marks the start of a gradual downhole transition in most physical properties (steeply increasing or decreasing trends) within Unit G2.

Unit G2 (47–71 mbsf) is considered a transitional geotechnical unit, defined by trends of decreasing bulk density and natural gamma radiation values and increasing water content; however, Unit G2 also exhibits high-amplitude fluctuations in these properties. This unit was defined in Hole 907A between 45 and 75 mbsf. This unit is poorly preserved in Hole 907B due to drilling disturbance in Core 162-907B-7H, but is preserved in Hole 907C. The lower boundary of Unit G2 in Hole 907B is placed just above a minimum in water content, which is observed in both Holes 907B (Fig. 20) and 907A (Fig. 21).

Low values of water content (or void ratio) and increased bulk density values at 60–64 mbsf may be associated with a hiatus in sedimentation or a condensed section in Hole 907B, according to shipboard paleomagnetic measurements (see "Paleomagnetism" section, this chapter). There are several ash layers within the corresponding interval in Hole 907A (Fig. 21), but this change in sedimentation rates was not noted by Myhre, Thiede, Firth, et al. (1995). Although this horizon (60–64 mbsf) could be interpreted as a geotechnical boundary, by locating the Unit G2 boundary at the base of the second large peak in water content (Fig. 20), our stratigraphy remains consistent between Holes 907A and 907B.

Geotechnical Unit G3 is defined from 71 to 193 mbsf, and is further divided in three subunits (Fig. 20; Table 19). There are subtle changes in the trends of all measured properties within Unit G3, but the unit is characterized by generally low values of bulk density (mean = 1.36 g/cm<sup>3</sup>) and high porosity values (mean = 79.26%) and water content (mean = 60.08%). Most properties, with the exception

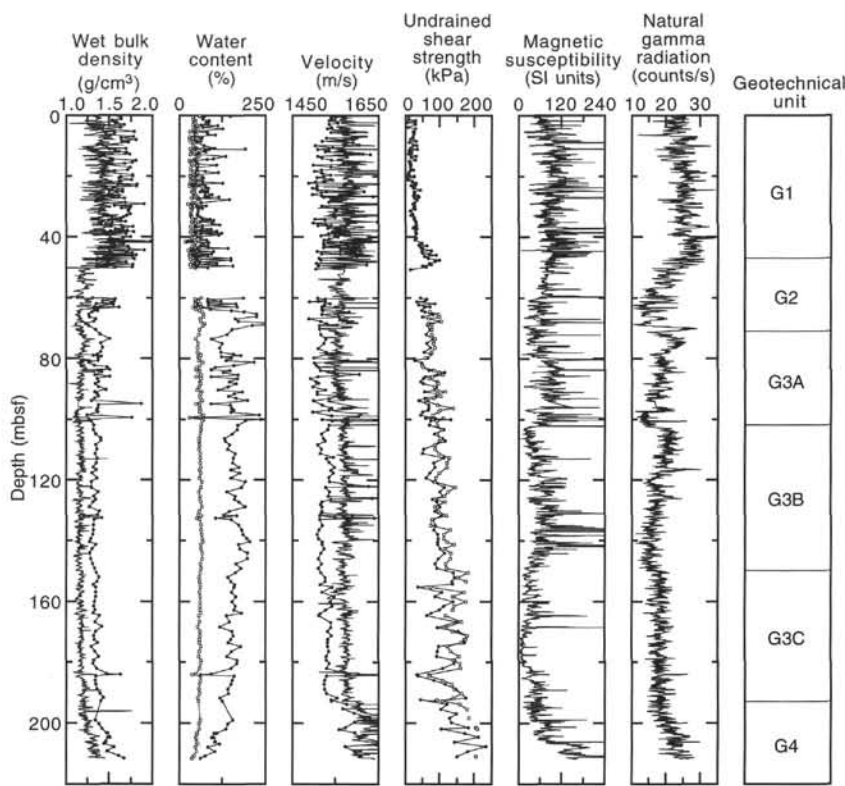


Figure 20. Plots of GRAPE wet bulk density (thin line) superimposed with gravimetric bulk density measurements (line with solid circles), water content (wt% wet sample = open squares; wt% dry sample = solid circles), PWL velocity (thin line) superimposed with split-core velocity (line with solid circles), undrained shear strength measured with the vane (solid circles) or the pocket penetrometer (open squares), magnetic susceptibility, and natural gamma radiation, vs. sub-bottom depth in Hole 907B. Also shown are the boundaries of geotechnical units.

Table 19. Mean values of physical properties for geotechnical units from Hole 907B.

Geotechnical unit:	G1	G2	G3	G3A	G3B	G3C	G4
Depth range (mbsf):	0–46	46–74	74–193	74–102	102–146	146–193	193–TD
Number of measurements:	110	32	104	35	34	35	14
Water content (% wet wt):	41.60	53.36	60.08	59.11	61.87	59.31	50.90
Water content (% dry wt):	74.77	129.04	154.51	151.04	164.32	148.46	106.47
Wet bulk density (g/cm <sup>3</sup> ):	1.63	1.46	1.36	1.38	1.33	1.36	1.48
Grain density (g/cm <sup>3</sup> ):	2.75	2.73	2.64	2.71	2.59	2.62	2.75
Dry bulk density (g/cm <sup>3</sup> ):	0.97	0.70	0.55	0.57	0.51	0.56	0.73
Porosity (%):	64.85	74.20	79.26	78.92	80.23	78.66	73.29
Void ratio:	2.01	3.44	3.98	4.01	4.15	3.80	2.85
Velocity (m/s):	1548 (106)	1535 (31)	1539 (109)	1546 (33)	1535 (40)	1536 (36)	1595 (13)
Vane shear strength (kPa):	27 (93)	64 (28)	91 (99)	68 (33)	92 (31)	113 (35)	155 (13)
Penetrometer (kPa):	NA	83 (10)	112 (92)	88 (28)	108 (31)	137 (33)	190 (6)
GRAPE density (g/cm <sup>3</sup> ):	1.41 (2512)	1.23 (1534)	1.18 (6505)	1.18 (1418)	1.17 (2369)	1.18 (2717)	1.29 (842)
Difference (WBD – GRAPE)	0.22	0.23	0.18	0.20	0.16	0.18	0.19

Notes: TD = total depth. For parameters other than index properties, the number of measurements used to calculate mean values are enclosed by parentheses. NA = not applicable.

of shear strength, show more variability in the first two subunits than in the third subunit of Unit G3.

Subunit G3A (74–102 mbsf) is defined by increasing trends in *P*-wave (PWL) velocity, porosity, and water content, and by decreasing trends in natural gamma radiation and bulk density (e.g., in both GRAPE density and gravimetric measurements) toward the base of the subunit. There are generally increased values of magnetic susceptibility within Subunit G3A, but decreased values of susceptibility are associated with both the upper and lower boundaries of the subunit. An increase in vane shear strength is also observed toward the lower boundary of this subunit. A possible condensed section or hiatus in sedimentation is indicated by magnetic measurements at about 98–100 mbsf (see “Paleomagnetism” section, this chapter), where higher velocities and additional changes in split-core measurements are observed.

Geotechnical Subunit G3B (102–150 mbsf) is defined by less variability and by gentler gradients in most properties than are ob-

served in Subunit G3A. Shear strength and water content values increase toward the base of the subunit, while natural gamma radiation decreases with depth. Bulk density (both GRAPE density and gravimetric measurements) and porosity values are nearly constant within this subunit, except for an interval between 130 and 134 mbsf, where a third possible condensed section or hiatus in sedimentation is indicated by magnetic measurements (see “Paleomagnetism” section, this chapter), and where abrupt changes in physical property values are observed. This horizon does not constitute a subunit boundary because the trends in MST data are not significantly modified by this discontinuity (Fig. 20). The Subunit G3B boundary at 150 mbsf is marked by an abrupt increase in shear strength. In Subunit G3C (150–193 mbsf), there are lower values of magnetic susceptibility compared to the overlying subunits, and a change to nearly constant or gently increasing values of natural gamma radiation, bulk density, and velocity. There is also higher variability in shear strength values in Subunit G3C.

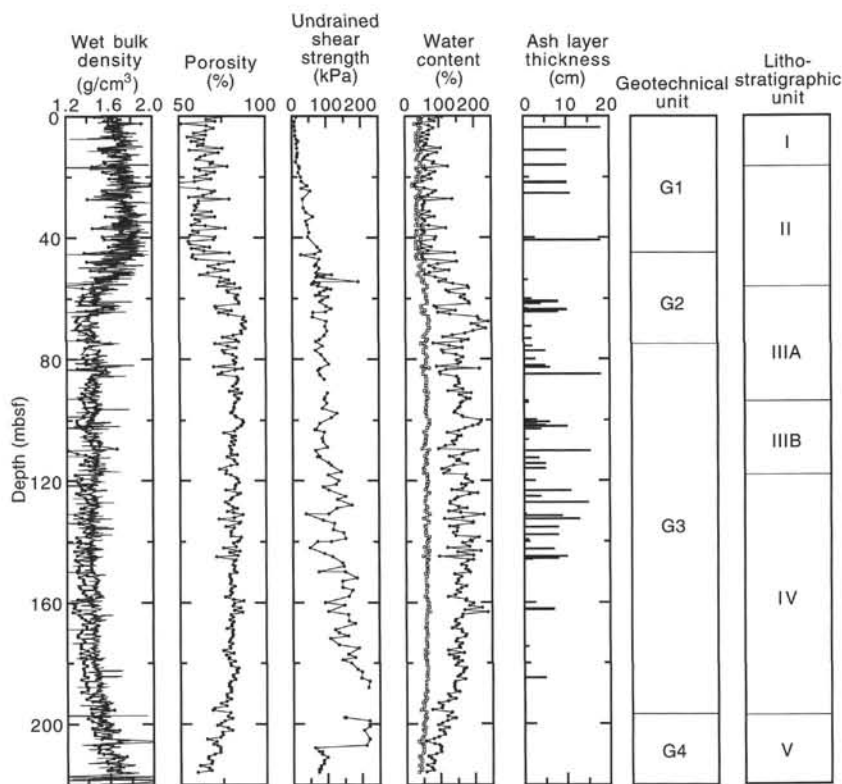


Figure 21. Plots of GRAPE wet bulk density (thin line) superimposed with gravimetric bulk density measurements (line with solid circles), porosity, average undrained shear strength, water content (wt% wet sample = squares; wt% dry sample = circles), and ash layer thickness, vs. sub-bottom depth in Hole 907A. Also shown are the boundaries of geotechnical and lithostratigraphic units (Myhre, Thiede, Firth, et al., 1995).

Geotechnical Unit G4 (from 193 mbsf to the limit of recovered sediment in Hole 907B) is defined by increasing trends in bulk density, shear strength, natural gamma radiation, magnetic susceptibility, and velocity, and by decreasing trends in water content and porosity (Fig. 20). The corresponding geotechnical unit in Hole 907A extends to the contact with the igneous rocks recovered at the base of that hole (see Myhre, Thiede, Firth, et al., 1995).

## Discussion

The boundaries of the geotechnical units described in this section are defined by reversals, inflections, and discontinuities in the down-hole trends of measured sediment index properties and on an analysis of the higher resolution data provided by sensors mounted on the MST. Lithostratigraphic unit boundaries are based on a somewhat different set of criteria, although the two methods seem to complement each other in describing the nature of the stratigraphic column at Site 907. In our geotechnical unit designations we have maintained the general format of what was proposed during Leg 151, but have used the additional constraints provided by the MST measurements of natural gamma radiation and *P*-wave velocity to divide geotechnical Unit G3 into three subunits.

The interbedded sediment layers between the mudline and about 47 mbsf, which comprise lithostratigraphic Unit I and the upper part of Unit II in Holes 907A and 907B, are nearly indistinguishable in terms of their bulk physical properties; therefore, this interval has been combined into a single geotechnical unit (G1). The fluctuations in physical properties within Unit G1 correspond to Pliocene to Quaternary lithologic variability associated with climatic (glacial-interglacial) cycles in the Northern Hemisphere (Myhre, Thiede, Firth, et al., 1995). Significant amounts of biogenic calcium carbonate are observed from the seafloor to 15.6 mbsf in Hole 907B (0–16.8 mbsf in Hole 907A).

Major changes in sediment texture and composition are suggested by the change in physical properties between geotechnical Units G1

and G3 in Hole 907A. The corresponding interval in Hole 907B is highly disturbed in Core 162-907B-7H, where discrete measurements were not made. In Hole 907B, the GRAPE density transition between Units G1 and G3 is much steeper than what is observed in the GRAPE record from Hole 907A. However, the natural gamma radiation record in Hole 907B is similar to the GRAPE density transition within Unit G2 of Hole 907A (Figs. 20, 21).

High-amplitude fluctuations in physical properties within Unit G2 are indicated by large increases and decreases in the relative amount of water in the sediment, which may reflect higher and lower abundances of clay minerals and/or increasing and decreasing amounts of biogenic silica in these sediments. Fluctuations in physical properties values were previously noted in Cores 151-907A-6H and 7H, where alternating textures (rough vs. smooth) in split cores were correlated with large amplitude fluctuations in GRAPE bulk density (Myhre, Thiede, Firth, et al., 1995). The significant decrease in bulk density in Unit G2, from about 1.8 g/cm<sup>3</sup> to about 1.5 g/cm<sup>3</sup> over the interval from 45 to about 60 mbsf, may reflect an increased ice-rafted-debris flux occurring simultaneously with the increased amplitude of oxygen isotope fluctuations from 3.1 to 2.6 Ma (Fronval and Jansen, in press; Shackleton et al., 1984). The high-amplitude fluctuations in density within this interval may be the expression of changes in the relative accumulation rates and/or composition of ice-rafted debris, clay minerals, and biogenic sediment during glacial or interglacial periods, possibly indicating cold/warm climatic oscillations superimposed on a gradual cooling trend (Jansen et al., 1988; Raymo, 1992).

The magnetic susceptibility record is highly variable in Hole 907B, but exhibits distinct minima near the boundaries and in the upper portions of geotechnical Subunits G3A and G3B, and within Subunit G3C. Similar magnetic susceptibility minima were observed in the record from Hole 907A, where they were attributed to either dilution by high biogenic (siliceous) sedimentation, and/or by a significant proportion of the magnetic material being destroyed by reductive diagenesis (Myhre, Thiede, Firth, et al., 1995). Intervals having reduced sedimentation rates or representing hiatuses in sedi-

mentation may be indicated at 60–64 mbsf, 98–100 mbsf (near the boundary between Subunits G3A and G3B), 130–134 mbsf, and at 184–186 mbsf according to the initial interpretation of the geomagnetic polarity reversal stratigraphy in Hole 907B (see “Paleomagnetism” section, this chapter), and a relationship between this and the magnetic susceptibility trend is therefore possible.

Intervals with relatively low natural gamma radiation are also located near the subunit boundaries of geotechnical Unit G3. These decreases in natural gamma radiation are often associated with peaks in water content and with changing trends in the magnetic susceptibility data (Fig. 20). These intervals may be characterized by changes in clay mineralogy, or by changes in the relative accumulation of biosiliceous material. Unit G4, in the lower portion of Site 907, is associated with an increase in silt-sized material and by indurated sedimentary layers above igneous rocks recovered in Hole 907A (Myhre, Thiede, Firth, et al., 1995).

#### REFERENCES

- Aagaard, K., and Carmack, E.C., 1994. The Arctic Ocean and climate: a perspective. In Johannessen, O.M., Muensch, R.D., and Overland, J.E. (Eds.), *The Role of the Polar Oceans in Shaping the Global Environment*. Geophys. Monogr., Am. Geophys. Union, 85:5–20.
- Aagaard, K., Swift, J.H., and Carmack, E.C., 1985. Thermohaline circulation in the Arctic Mediterranean seas. *J. Geophys. Res.*, 90:4833–4846.
- Berggren, W.A., Hilgen, F.J., Langereis, C.G., Kent, D.V., Obradovich, J.D., Raffi, I., Raymo, M.E., and Shackleton, N.J., 1995. Late Neogene chronology: new perspectives in high-resolution stratigraphy. *Geol. Soc. Am. Bull.*, 107:1272–1287.
- Berner, R.A., 1984. Sedimentary pyrite formation: an update. *Geochim. Cosmochim. Acta*, 48:605–615.
- Cande, S.C., and Kent, D.V., 1995. Revised calibration of the geomagnetic polarity timescale for the Late Cretaceous and Cenozoic. *J. Geophys. Res.*, 100:6093–6095.
- Eide, L., Beyer, I., and Jansen, E., in press. Comparison of Quaternary interglacial periods in the Iceland Sea. *J. Quat. Sci.*
- Eldholm, O., Thiede, J., Taylor, E., et al., 1987. *Proc. ODP, Init. Repts.*, 104: College Station, TX (Ocean Drilling Program).
- Eldholm, O., Thiede, J., and Taylor, E., 1989. Evolution of the Vøring volcanic margin. In Eldholm, O., Thiede, J., Taylor, E., et al., *Proc. ODP, Sci. Results*, 104: College Station, TX (Ocean Drilling Program), 1033–1065.
- Eldholm, O., and Windisch, C.C., 1974. Sediment distribution in the Norwegian-Greenland Sea. *Geol. Soc. Am. Bull.*, 85:1661–1676.
- Fronval, T. and Jansen, E., in press. Late Neogene paleoclimates and paleoceanography in the Iceland-Norwegian Sea: evidence from the Iceland and Vøring Plateaus, ODP Leg 151 and 104. In Myhre, A., Thiede, J., Firth, J. et al., *Proc. ODP, Sci. Results*, 151: College Station, TX (Ocean Drilling Program).
- Henrich, R., and Baumann, K.H., 1994. Evolution of the Norwegian Current and the Scandinavian Ice Sheets during the past 2.6 m.y.: evidence from ODP Leg 104 biogenic carbonate and terrigenous records. *Palaeogeogr., Palaeoclimatol., Palaeoecol.*, 108:75–94.
- Imbrie, J., Boyle, E.A., Clemens, S.C., Duffy, A., Howard, W.R., Kukla, G., Kutzbach, J., Martinson, D.G., McIntyre, A., Mix, A.C., Molfino, B., Morley, J.J., Peterson, L.C., Pisias, N.G., Prell, W.L., Raymo, M.E., Shackleton, N.J., and Toggweiler, J.R., 1992. On the structure and origin of major glaciation cycles, 1. Linear responses to Milankovitch forcing. *Paleoceanography*, 7:701–738.
- , 1993. On the structure and origin of major glaciation cycles, 2. The 100,000-year cycle. *Paleoceanography*, 8:699–736.
- Jansen, E., Bleil, U., Henrich, R., Kringstad, L., and Slettemark, B., 1988. Paleoenvironmental changes in the Norwegian Sea and Northeast Atlantic during the last 2.8 m.y.: Deep Sea Drilling Project/Ocean Drilling Program Sites 610, 642, 643, and 644. *Paleoceanography*, 3:563–581.
- Koç, N., and Jansen, E., 1994. Response of high latitude Northern Hemisphere to orbital climate forcing: evidence from the Nordic Seas. *Geology*, 22:523–526.
- Leventhal, J.S., 1983. An interpretation of carbon and sulfur relationships in Black Sea sediments as indicators of environments of deposition. *Geochim. Cosmochim. Acta*, 47:133–137.
- Locker, S., and Martini, E., 1989. Cenozoic silicoflagellates, ebridians, and actiniscidians from the Vøring Plateau (ODP Leg 104). In Eldholm, O., Thiede, J., Taylor, E., et al., *Proc. ODP, Sci. Results*, 104: College Station, TX (Ocean Drilling Program), 543–585.
- McDuff, R.E., 1981. Major cation gradients in DSDP interstitial waters: the role of diffusive exchange between seawater and upper oceanic crust. *Geochim. Cosmochim. Acta*, 45:1705–1713.
- Myhre, A.M., Thiede, J., Firth, J.V., et al., 1995. *Proc. ODP, Init. Repts.*, 151: College Station, TX (Ocean Drilling Program).
- Okada, H., and Bukry, D., 1980. Supplementary modification and introduction of code numbers to the low-latitude coccolith biostratigraphic zonation (Bukry, 1973; 1975). *Mar. Micropaleontol.*, 5:321–325.
- Peters, K.E., 1986. Guidelines for evaluating petroleum source rock using programmed pyrolysis. *AAPG Bull.*, 70:318–329.
- Raymo, M.E., 1992. Global climate change: a three million year perspective. In Kukla, G.J., and Went, E. (Eds.), *Start of a Glacial*. NATO ASI Ser., 13: Berlin (Springer-Verlag), 207–223.
- Schrader, H.-J., and Fenner, J., 1976. Norwegian Sea Cenozoic diatom biostratigraphy and taxonomy. In Talwani, M., Udintsev, G., et al., *Init. Repts. DSDP*, 38: Washington (U.S. Govt. Printing Office), 921–1099.
- Shackleton, N.J., Backman, J., Zimmerman, H., Kent, D.V., Hall, M.A., Roberts, D.G., Schnitker, D., Baldauf, J.G., Desprairies, A., Homrighausen, R., Huddleston, P., Keene, J.B., Kaltenback, A.J., Krumsiek, K.A.O., Morton, A.C., Murray, J.W., and Westberg-Smith, J., 1984. Oxygen isotope calibration of the onset of ice-rafting and history of glaciation in the North Atlantic region. *Nature*, 307:620–623.
- Shipboard Scientific Party, 1995. Site 907. In Myhre, A.M., Thiede, J., Firth, J.V., et al., *Proc. ODP, Init. Repts.*, 151: College Station, TX (Ocean Drilling Program), 57–111.
- Stein, R., 1990. Organic carbon/sedimentation rate relationship and its paleoenvironmental significance for marine sediments. *Geo-Mar. Lett.*, 10:37–44.
- , 1991. *Accumulation of Organic Carbon in Marine Sediments: Results from the Deep Sea Drilling Project/Ocean Drilling Program (DSDP/ODP)*. Lect. Notes Earth Sci., 34: Berlin (Springer-Verlag).
- Talwani, M., and Eldholm, O., 1977. Evolution of the Norwegian-Greenland Sea. *Geol. Soc. Am. Bull.*, 88:969–999.
- van Andel, T.H., Heath, G.R., and Moore, T.C., Jr., 1975. Cenozoic history and paleoceanography of the central equatorial Pacific Ocean: a regional synthesis of Deep Sea Drilling Project data. *Mem.—Geol. Soc. Am.*, 143.
- Weaver, P.P.E., and Clement, B.M., 1986. Synchronicity of Pliocene planktonic foraminiferal datums in the North Atlantic. *Mar. Micropaleontol.*, 10:295–307.

Ms 162IR-107

**Note:** For all sites drilled, core description forms (“barrel sheets”) and core photographs can be found in Section 3, beginning on page 391. Forms containing smear slide data can be found in Section 4, beginning on page 1147. On the CD-ROM enclosed in the back pocket of this volume are all tables from this chapter (including an extended coring summary table) and shipboard measurements (files containing GRAPE density, P-wave velocity, natural gamma radiation, magnetic susceptibility, index properties, and spectral reflectance data).